



## Invited Review Paper

# Vibration control based metamaterials and origami structures: A state-of-the-art review



J.C. Ji\*, Quantian Luo, Kan Ye

School of Mechanical and Mechatronic Engineering, University of Technology Sydney, NSW 2007, Australia

## ARTICLE INFO

*Article history:*

Received 29 November 2020

Received in revised form 3 March 2021

Accepted 3 April 2021

Communicated by: John E Mottershead

*Keywords:*

Vibration control

Metamaterials

Origami-based Structures

Vibration Isolation

Quasi-zero-stiffness

## ABSTRACT

Vibration and sound control is critical to many practical engineering systems in order to minimise the detrimental effects caused by unavoidable vibrations and noises. Metamaterials and origami-based structures, which have attracted increasing interests in interdisciplinary research fields, possess many peculiar physical properties, including negative Poisson's ratios, bi- or multi-stable states, nonlinear and tuneable stiffness features, and thus offer promising applications for vibration and sound control. This paper presents a review of metamaterials and origami-based structures as well as their applications to vibration and sound control. Metamaterials are artificially engineered materials having extremal properties which are not found in conventional materials. Metamaterials with abnormal features are firstly discussed on the basis of the unusual values of their elastic constants. Recent advances of auxetic, band gap and pentamode metamaterials are reviewed together with their applications to vibration and sound mitigations. Origami, as the ancient Japanese art of paper folding, has emerged as a new design paradigm for different applications. Origami-based structures can be adopted for vibration isolation by using their multi-stable states and desirable stiffness characteristics. Different origami patterns are reviewed to show their configurations and base structures. Special features, such as bi- or multi-stable states, dynamic Poisson's ratios, and nonlinear force-displacement relationships are discussed for their applications for vibration control. Finally, possible future research directions are elaborated for this emerging and promising interdisciplinary research field.

© 2021 Elsevier Ltd. All rights reserved.

## Contents

1. Introduction . . . . .	2
1.1. Vibration isolation. . . . .	3
1.2. Mechanical metamaterials . . . . .	3
1.3. Origami-based structures . . . . .	4
2. Mechanical and acoustic metamaterials . . . . .	5
2.1. Classification of metamaterials. . . . .	6
2.1.1. The Milton map . . . . .	6
2.1.2. Optical and electro-magnetic metamaterials . . . . .	7
2.1.3. Acoustic metamaterials . . . . .	7

\* Corresponding author.

E-mail addresses: [jin.ji@uts.edu.au](mailto:jin.ji@uts.edu.au) (J.C. Ji), [quantian.luo@uts.edu.au](mailto:quantian.luo@uts.edu.au) (Q. Luo), [kan.ye@uts.edu.au](mailto:kan.ye@uts.edu.au) (K. Ye).

2.1.4. Pentamode materials . . . . .	8
2.1.5. Analogue to band gap. . . . .	8
2.1.6. Nonlinear stress-strain and force-displacement relationships . . . . .	9
2.2. Cellular structures . . . . .	9
2.2.1. The Hashin-Shtrikman bounds . . . . .	9
2.2.2. Cellular structures . . . . .	10
2.2.3. Nonlinear property for vibration isolation . . . . .	12
2.3. Auxetic metamaterials . . . . .	12
2.3.1. Poisson's ratio. . . . .	12
2.3.2. Re-entrant honeycomb metamaterials . . . . .	13
2.3.3. Auxetic property, damping, energy absorption and dissipation . . . . .	14
2.4. Band gap metamaterials . . . . .	14
2.4.1. Approaches of band gap metamaterials to attenuate wave propagation . . . . .	15
2.4.2. Locally resonant sub-structures. . . . .	15
2.4.3. Linear band gap acoustic metamaterials and applications. . . . .	17
2.4.4. Nonlinear band gap metamaterials . . . . .	17
2.5. Pentamode metamaterials . . . . .	18
2.5.1. Structures of pentamode materials . . . . .	18
2.5.2. Property of pentamode metamaterials . . . . .	18
2.5.3. Fabrication and application to vibration and sound control . . . . .	19
3. Origami-based structures. . . . .	21
3.1. Common crease patterns and folding parameters. . . . .	21
3.1.1. Generic degree-4 vertex pattern . . . . .	21
3.1.2. Miura-ori pattern . . . . .	21
3.1.3. Stacked Miura-ori pattern . . . . .	23
3.1.4. Tachi-Miura polyhedron pattern. . . . .	23
3.1.5. Waterbomb base. . . . .	23
3.1.6. Cylindrical pattern and the other patterns . . . . .	24
3.2. Design of origami structures . . . . .	24
3.2.1. Crease design . . . . .	24
3.2.2. Facet design . . . . .	25
3.2.3. Kinematic modelling . . . . .	26
3.3. Dynamic modelling and vibration control. . . . .	27
3.3.1. Dynamic behaviour . . . . .	27
3.3.2. Origami-based QZS isolator . . . . .	28
3.4. Fabrication of origami structures . . . . .	31
4. Concluding remarks . . . . .	31
4.1. Summary . . . . .	31
4.2. Challenges and further work . . . . .	31
4.2.1. Nonlinear analysis and negative properties . . . . .	31
4.2.2. Fabrication, nano-scale and size effect, and test. . . . .	32
4.2.3. Topology optimization and 3D metamaterials. . . . .	32
4.2.4. Smart metamaterials and origami-based structures . . . . .	32
4.2.5. Novel design and realization of origami-based structures. . . . .	32
Declaration of Competing Interest . . . . .	33
Acknowledgments . . . . .	33
References . . . . .	33

## 1. Introduction

Vibration and sound control is essential and critical to many engineering applications in order to minimize the undesirable and harmful effects caused by unavoidable vibrations and noises. Use of metamaterials and origami-based structures for vibration control and sound mitigation has attracted increasingly interests due to their specific properties, including negative and varying Poisson's ratios, nonlinear force-displacement relationships, bi- or multi-stable states, the ability to absorb vibration energy, negative bulk modulus and negative refractive index. Metamaterials with various cell structures and origami-based structures with different patterns have been recently designed to exhibit negative stiffness feature, nonlinear shear modulus under large deformation, and quasi-zero dynamic stiffness, which are very promising for vibration control and sound absorption.

Metamaterials and origami-based structures seem to be two different concepts from their names. However, they have shown some inseparable relationships in that the terms such as origami metamaterials, origami-inspired metamaterials, and origami-based mechanical metamaterials have been widely used in the literature. In this review paper, we try to separate these two concepts by discussing metamaterials from the perspective of mechanical properties and origami structures from a structure viewpoint, though a complete separation is impossible.

### 1.1. Vibration isolation

The passive vibration control can be realized by using tuned vibration absorbers, tuned mass dampers, linear and nonlinear vibration isolators. Vibration isolation, as one of the most commonly adopted vibration mitigation methods, prevents vibrations transferred to an object by isolating the object from the source of vibrations. Linear vibration isolators have been widely used in many engineering applications, but they are effective only when their natural frequencies are well below the excitation frequency. To overcome this shortcoming, nonlinear vibration isolators with high-static and low-dynamic stiffness characteristics have been designed to isolate the vibrations in low frequency range (for example, [1–9]). Here, high-static stiffness component implies large load-carrying capacity, while the low-dynamic stiffness component means an increased isolation region. A nearly zero dynamic stiffness component at the operating point, as the distinctive feature of the nonlinear isolators, has been referred to as quasi-zero stiffness (QZS) characteristics in the literature, and nonlinear isolators with QZS characteristics will be referred to here as *QZS isolators*. Negative stiffness (NS) elements play a vital role in forming the QZS feature by counteracting positive stiffness structures. The NS feature can be realized from different structures, such as oblique springs [2,10–12], buckling beams [13], bi-stable structures [14–19], magnet springs [20–23], and bio-inspired structures [24–26]. Different types of the NS structures can be used either individually or in a combination.

For metamaterials, the NS behavior can be realized by incorporating a NS metamaterial unit cell or NS-substructure/element. The metamaterials with a unit cell comprised of one negative and two positive stiffness elements was designed in [19] to induce hysteresis in a loading–unloading cycle, leading to significant energy dissipation. Metamaterials with NS elements could also achieve good cushion performance when the snap-through behavior occurs [18]. Repeated experiments showed that the bi-stable and multi-stable structures could be reusable even though large deformations occurred under cyclic loading [27–30]. Metamaterials comprised of periodic cells with bi-stable states and phase transformations can exhibit hysteresis and thus they are attractive for energy absorption in vibration alleviation [31–33].

Metamaterials with peculiar features, such as negative stiffness, bi-stable states, high energy dissipation, and high damping ratios, could effectively mitigate vibration and sound wave propagation, for example, a thin-film acoustic metamaterial comprised of an elastic membrane and asymmetric rigid platelets to absorb low-frequency airborne noise in selective resonance frequencies [34], wave-guide piezoelectro-mechanical metamaterials to control wave propagation [35], re-entrant hexagonal honeycombs under large deformation to dissipate dynamic energy [36], and nanolattice mechanical metamaterials with ultrahigh strength and stiffness to absorb energy [37]. Generally, auxetic metamaterials with negative Poisson's ratios can efficiently absorb and dissipate dynamic energy. Band gap metamaterials may block stress waves with a specific frequency band and pentamode metamaterials with near zero shear moduli can attenuate shear wave propagation.

### 1.2. Mechanical metamaterials

Metamaterials have been increasingly receiving research interests over the last two decades because they exhibit extraordinary optical, electromagnetic, acoustic and mechanical characteristics that are different from conventional materials [38,39]. Metamaterial properties change with their substructures rather than with composition and their peculiar physical properties are not found in nature. Artificially constructed metamaterials are engineered by constructing multiple individual elements or cells and can demonstrate behaviors similar to those of functional graded materials. Multiple elements or cells in metamaterials are often arranged in periodic patterns, akin to cellular structures, and their specific performance can be studied from a unit cell. In general, scales of the unit cells in metamaterials are normally less than wavelength of the influenced property.

Metamaterials with peculiar electromagnetic, optical or thermodynamic properties such as negative refractive index and abnormal field constants were firstly designed and fabricated for cloaking objects and filtering optical and electromagnetic waves [39–43]. In analogy to phononic structures in electromagnetic and optical metamaterials, metamaterials with unusual mechanical and acoustic properties have received considerable attention [29,44–48]. Mechanical and acoustic metamaterials include but not limited to cellular metamaterials [49], origami-inspired metamaterials, materials with band gap property [50–52], auxetic metamaterials with negative Poisson's ratios [53–55], pentamode metamaterials with significantly higher bulk modulus than shear modulus [56–58], and origami-based mechanical metamaterial structures [59–62]. Band gap metamaterials filtering stress waves, cellular structures with negative stiffness elements, auxetic materials absorbing high energy and pentamode materials blocking shear waves are promising metamaterials for vibration and sound control.

Phononic crystal and electromagnetic metamaterials were originally studied in the early research on periodic systems by Newton and Rayleigh. In analogy to an electronic band diagram and atomic crystal lattice structures, acoustic metamaterials were then developed [63–68] for controlling sound waves in a way that is impossible in conventional materials. Rapid development of mechanical metamaterials in the last few years results from the advances in additive manufacturing techniques so that metamaterials with arbitrarily complex micro/nano-architectures could be manufactured. Metamaterials with zero or

even negative refractive index can provide possibilities for sound control at subwavelength scales [69]. Metamaterials with extremal properties such as pentamode, dilational, auxetic and bio-inspired metamaterials offer new possibilities for vibration control and sound absorption [46,48,70–73].

Metamaterials created on the basis of origami element (unit cell) with a periodic Miura-ori pattern and a non-periodic Ron Resch pattern provide foundations to design origami-based metamaterials [74]. In this type of metamaterials, extraordinary coexistence of positive and negative Poisson's ratios for in-plane and out-of-plane deformations was reported [74,75]. In the Miura-ori tessellation based metamaterials, the unit cell of this crease pattern is mechanically bistable and can be tuned by switching between deploying and folding states [76,77]. This enables origami-based metamaterials to provide bi-stable and multi-stable states [60,61]. With this characteristic, origami-based metamaterials can be efficiently used to store and dissipate dynamic energy for vibration attenuation [62].

### 1.3. Origami-based structures

Origami originally refers to the ancient Japanese art of paper folding. The word *origami* is a compound formed from two Japanese words, *ori* meaning to fold (or folding), and *kami* meaning *paper*. At the early stage, origami was mainly for recreational and artistic purpose, rather than engineering applications [78]. Appropriate design of origami base elements (unit cells) and different crease patterns can form desired origami structures [79–81] and complicated configurations [82]. Origami-based structures are also known as a special type of morphing structures. Origami base elements (or base structures) usually have two stable states, namely folding and expanding states [83] and origami structures can produce many unique mechanical properties, such as shape configurations, auxetic properties, multi-stability, nonlinear and tuneable stiffness [59].

Morphing structures have found their wide applications in practical engineering areas such as aircraft [84] and wind turbines [85]. Origami structures have shown their advantages over other morphing structures [76,86], including compact deployment, storage capability, re-configurability ability, bi- and multi-stable states. Origami-based structures can be stored in a small size when folding and used in a full size when deploying. By taking these advantages, various origami-based structures have been proposed for practical engineering applications, such as collapsible kayaks [87], pneumatic actuators [88], space telescope lenses [89], conceal-and-reveal box [90], oriceps [91], energy absorption devices [92,93], medical devices [94–96], actuators used in soft robots [97]. The multi-stable behaviours of the origami-based structure can switch among different stable states to reduce complexity of the control architecture for improving the robot locomotion [98,99].

The main characteristics of origami structures, which can be used for vibration isolation, include foldability, multi-stability, nonlinear and tuneable stiffness.

**Foldability:** Foldability includes rigid-foldability and flat-foldability, where rigid-foldability refers to a crease pattern which is rigid-foldable, and flat-foldability is a property enabling the paper (sheet) to be folded into a single plane (folded flat) without collisions of the parts. The early origami structure is a folded paper whose three-dimensional (3D) shape can be constructed by folding a two-dimensional (2D) paper sheet. The facets are folded along the creases in opposite directions to form either mountain or valley. Two states of the origami structure can be switched between 3D folded configuration and 2D unfolded shape.

**Multi-stability:** An origami base structure has bi-stable states and the formed origami structures can possess multiple stable configurations from one-to-many mapping in geometric relations. Multi-stability of origami structures originates from the multiple stable states. Bi-stability of the origami structure does not require the continuous actuation to hold its stable configurations [100]. There could be up to six distinct energy branches when folding from the flat state [101,102]. Each stable state could be considered as an operating position for vibration isolation.

**Nonlinear stiffness:** Origami structures can be generated by designing crease patterns and facets, and their overall kinematics can be expressed as a function of the folding deformation of the creases and the bending of the facets. The resultant geometric nonlinearities associated with folding patterns lead to nonlinear force-displacement relationships, thereby providing nonlinear stiffness. For example, the origami cellular structures could exhibit the nonlinear stiffness in multi-directions [103]. The nonlinear stiffness feature would enable origami structures to meet the requirements of vibration isolation in different applications.

Force analysis method has been commonly used in designing QZS isolators, and the corresponding force-displacement relationships can be easily uncovered through analysing the geometric relationships of the QZS mechanical structures. However, for complex metamaterials and origami structures with hierarchical interactions, energy analysis method has been used to study the energy absorbing or shielding abilities, avoiding the difficulty in analysing deformation mechanisms to obtain force-displacement relationships. Calculation of energy landscape of the proposed origami structures could provide valuable insights for their ability as energy absorbing or shielding, which open potential applications to vibration and sound control.

There are massive and diverse literature in interdisciplinary disciplines covering a broad range of metamaterials, origami structures, and their applications for vibration and sound control. Omission of some papers in these areas could not be avoided, though unfortunately. This paper is to present a review on metamaterials and origami structures coherently related to vibration and sound control. The remaining of this paper is organized as follows. Abnormal properties of metamaterials are first discussed in Section 2.1, and then cellular structures, materials with negative Poisson's ratio, band gap and pentamode metamaterials are reviewed in Sections 2.2–2.5, respectively. Section 3 is composed of four subsections, which discuss

the common crease patterns of origami structures, design of origami structures, dynamic modelling and vibration control, as well as the fabrication of origami structures, respectively. Conclusion and prospective research are given in [Section 4](#).

## 2. Mechanical and acoustic metamaterials

Metamaterials made of micro-architectures can offer the desired mechanical properties dependent on their micro-scale structures. As metamaterials consist of periodically arranged cells, their mechanical properties can be studied based on a unit cell. A simple way of studying their mechanical properties is to find their effective material constants via homogenization for the unit cell. The homogenized behaviors of metamaterials resemble those of the unit cell structures. The homogenized macro-scale properties highly depend on the micro-scale structure that could be designed so that the resulting metamaterials have unusual values of physical and mechanical properties.

[Fig. 1\(a\)](#) shows multi-scale properties of materials. In an atomic scale, material properties may be described by  $\alpha_i$  and  $\beta_i$ , where  $\alpha_i$  and  $\beta_i$  represent the stretching and bending deformations of valence bonds of atoms caused by Van der Waals (VdW) force [104]. In a single crystal,  $C_{ij}$  denotes the crystal coefficients. In a macro scale or engineering, material properties are usually represented by elastic constants. Metamaterials with unusual, rare or extraordinary elastic mechanical properties include linear elastic behaviors described by an elastic constant matrix and nonlinear feature due to large deformation described by stress-strain or force-displacement relationships.

In linear analysis, the constitutive equation of elastic anisotropic materials is written as [105]:

$$\sigma_{ij} = C_{ijkl}\varepsilon_{kl}; \quad (i, j, k, l = 1, 2, \dots, 6) \quad (1)$$

where  $\sigma_{ij}$  and  $\varepsilon_{kl}$  are the stress and strain tensors, and  $c_{ijkl} = c_{klji}$  denote the elastic constants of materials.

For the isotropic materials, Eq. (1) can be expressed as:

$$\begin{Bmatrix} \varepsilon_x \\ \varepsilon_y \\ \varepsilon_z \end{Bmatrix} = \frac{1}{E} \begin{bmatrix} 1 & -\nu & -\nu \\ -\nu & 1 & -\nu \\ -\nu & -\nu & 1 \end{bmatrix} \begin{Bmatrix} \sigma_x \\ \sigma_y \\ \sigma_z \end{Bmatrix} \quad (2a)$$

$$\begin{Bmatrix} \gamma_{xy} \\ \gamma_{yz} \\ \gamma_{zx} \end{Bmatrix} = \frac{1}{G} \begin{bmatrix} 1 & 0 & 0 \\ 0 & 1 & 0 \\ 0 & 0 & 1 \end{bmatrix} \begin{Bmatrix} \tau_{xy} \\ \tau_{yz} \\ \tau_{zx} \end{Bmatrix} \quad (2b)$$

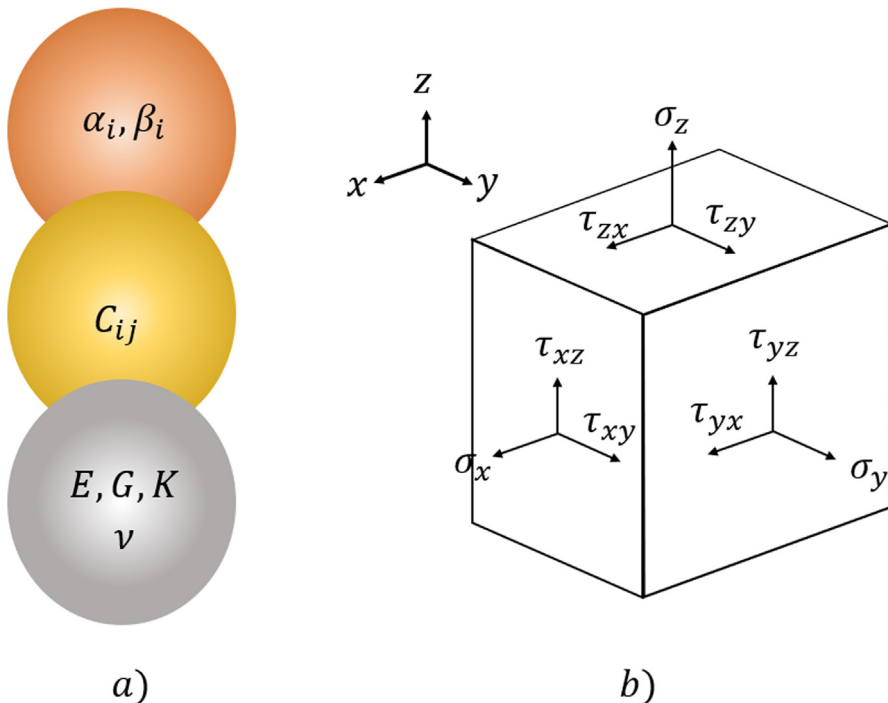


**Fig. 1.** Constitutive relations of materials: (a) multi-scale description, (b) isotropic materials.

where  $\varepsilon$  and  $\gamma$  represent the normal and shear strains,  $E$  and  $G$  denote Young's modulus and shear modulus,  $v$  stands for Poisson's ratio,  $\sigma$  and  $\tau$  are the normal and shear stresses, as shown in Fig. 1(b).

Adding the three equations of Eq. (2a) and then performing some algebraic manipulations yields:

$$\theta = \frac{1}{K} \sigma_m \quad (3)$$

in which

$$\theta = \varepsilon_x + \varepsilon_y + \varepsilon_z \quad (4a)$$

$$K = \frac{E}{3(1 - 2v)} \quad (4b)$$

$$\sigma_m = \frac{1}{3} (\sigma_x + \sigma_y + \sigma_z) \quad (4c)$$

where  $\theta$  denotes the volume change,  $K$  is the bulk modulus, and  $\sigma_m$  represents the average stress or the octahedral normal stress.

When an infinitesimal element shown in Fig. 1(b) is subjected to stresses, its volume and shape will be changed. Strain energy densities for the volume and shape changes can be expressed as:

$$u_v = \frac{1}{2K} \sigma_m^2 = \frac{1}{2} K \theta^2 \quad (5)$$

$$u_s = \frac{1+v}{6E} [(\sigma_1 - \sigma_2)^2 + (\sigma_2 - \sigma_3)^2 + (\sigma_3 - \sigma_1)^2] = \frac{3}{4G} \tau_{oct}^2 \quad (6)$$

where  $\sigma_1$ ,  $\sigma_2$  and  $\sigma_3$  are the principal stresses, and  $\tau_{oct}$  denotes the octahedral shear stress. In Eq. (6), the following relationship of  $E$ ,  $G$  and  $v$  has been used:

$$G = \frac{E}{2(1+v)} \quad (7)$$

By using Eqs. (4b) and (7), the following relationships can be derived:

$$E = \frac{9KG}{3K+G} \quad (8)$$

$$v = \frac{3K-2G}{2(3K+G)}, \text{ Or } \frac{K}{G} = \frac{2(1+v)}{3(1-2v)}$$

In linear analysis for isotropic materials, material properties are characterized by Young's modulus  $E$ , shear modulus  $G$ , bulk modulus  $K$ , and Poisson's ratio  $v$ . These elastic constants are respectively associated with stiffness, rigidity, compressibility and auxeticity of materials.

## 2.1. Classification of metamaterials

Metamaterials can be grouped according to their general mechanical properties. For different purposes, metamaterials can be designed to have unique features.

### 2.1.1. The Milton map

It can be seen from Eqs. (5) and (6) that bulk modulus  $K$  reflects the volume expansion deformation and shear modulus  $G$  is related to the shape deformation. When  $K$  and  $G$  are assumed to be positive to ensure materials thermodynamically stable, elastic tensor  $c_{ijkl}$  is positively definite and  $E$  is also positive based on Eq. (8). A thermodynamically admissible value range of Poisson's ratio can be obtained as  $-1 < v < 0.5$  on the basis of Eqs. (7) and (9). In general, Poisson's ratio is in a range of  $0 < v < 0.5$  for most of natural solids and many normal engineering materials have Poisson's ratios of  $v = 0.25 \sim 0.35$ . When  $v = 0.25 \sim 0.35$ ,  $K/G = 1.67 \sim 3$  can be calculated by Eq. (9), which means that the magnitudes of bulk and shear moduli are comparable. In the Milton map, also referred to as the  $K - G$  map, these materials locate between two lines shown in Fig. 2 [104,106]. The Milton map is often used to show relationships of bulk modulus and shear modulus. In the vertical axis,  $v = 0.5$ , indicates the material possesses liquid feature, which is the pentamode material. In the horizontal axis,  $v = -1$ , denotes the extremal case of auxetic materials. When  $-4G/3 < K < 0$ , the materials have negative compressibility.

The peculiar phenomena of metamaterials are categorized by abnormal value ranges and the combinations of these constants. As Poisson's ratio  $v$  approaches 0.5, shear modulus approaches zero or  $K \gg G$ . This type of metamaterials may be regarded as an ideal fluid as the materials can easily flow under shear stress. Two types of metamaterials can behave this property, namely, pentamode metamaterials [107] and the mechanical metamaterials with a kagome lattice, as shown in

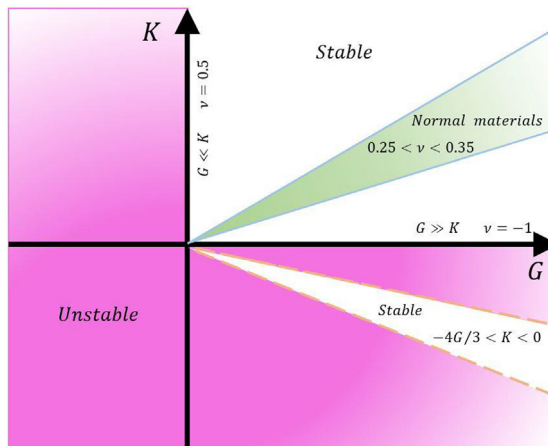


**Fig. 2.** The Milton map, relationships of bulk and shear moduli with Poisson's ratio.

**Fig. 3.** When Poisson's ratio  $\nu$  approaches  $-1$ ,  $K \ll G$ . Materials with tailorable Poisson's ratio are referred to as auxetic materials shown in Fig. 4 [48,108], and natural cork is an example of the material with zero Poisson's ratio.

### 2.1.2. Optical and electro-magnetic metamaterials

Smith et al. [39] reviewed metamaterials with negative refractive index and indicated that metamaterials in nano-scale with artificial magnetism and negative refractive index were two specific behaviors. Pendry et al. [42] showed that the electromagnetic fields of metamaterials could be redirected at will by controlling electromagnetic fields. They also illustrated the cloaking that could exclude all electromagnetic fields. Cai et al. [43] indicated that artificial metamaterials could enable unprecedented flexibility in manipulating electromagnetic waves and could produce the cloak of invisibility. Valentine et al. [109] studied the metamaterials with spatially tailored properties to provide the necessary medium by enabling precise control over the flow of electromagnetic waves and demonstrated an optical cloak made of isotropic dielectric materials, which enabled broadband and low-loss invisibility at a nanoscale wavelength range.

### 2.1.3. Acoustic metamaterials

Phononic crystal metamaterials were proposed about two decades ago and some important characteristics such as acoustic band gap and negative refraction have motivated fundamental studies in acoustic materials since then. Lu et al. [64] showed that acoustic metamaterials with their inherent subwavelength nature could achieve negative bulk modulus and/or negative mass density by carefully designing a phononic crystal in an acoustic scale.

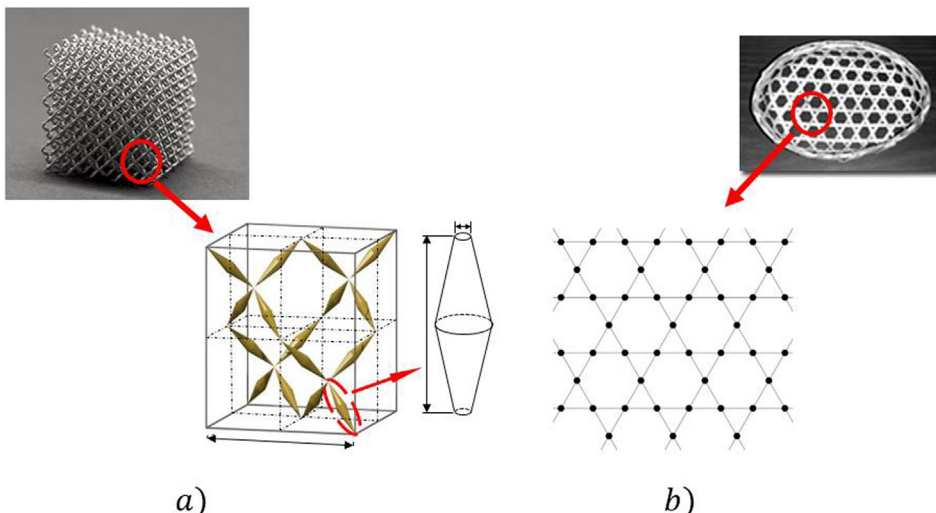


**Fig. 3.** Metamaterials with very small shear modulus: (a) pentamode metamaterials, (b) metamaterials with a kagome lattice.

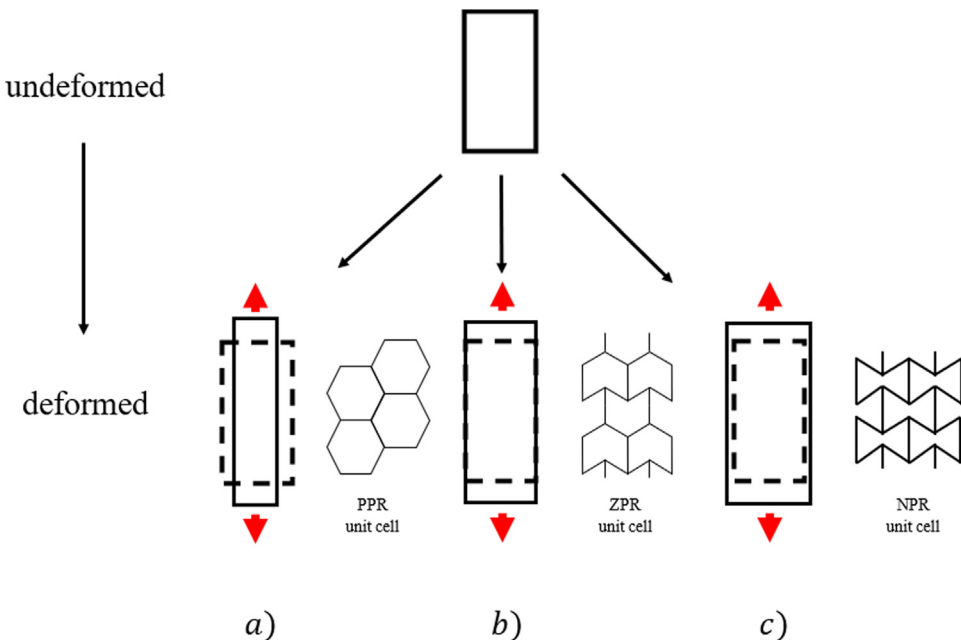


**Fig. 4.** Metamaterials with tailorable Poisson's ratios: (a) positive Poisson's ratio (PPR), (b) approximate zero Poisson's ratio (ZPR), and (c) negative Poisson's ratio (NPR). Examples of typical unit cells are given on the sides.

A great challenge in designing composite metamaterials is the ability to fabricate materials that simultaneously exhibit high stiffness and high loss factor for the creation of structural elements capable of suppressing vibration and/or acoustic energy. Metamaterials whose macroscopic mechanical stiffness and loss factor surpass those of conventional materials could be produced through adding materials with NS feature induced by phase transformation [110]. Klatt and Haberman [111] investigated the NS behaviors using the controlled buckling of small-scale structural elements that were embedded in a continuous viscoelastic matrix rather than utilizing physical phenomena such as inherent nonlinear material behavior or dynamic effects.

Haberman and Guild [44] presented a review on acoustic metamaterials and indicated that many acoustic metamaterial devices often required strange concepts such as negative density and negative compressibility. Since the early 21st century, acoustic metamaterials have emerged from academic curiosity to become an active field driven by scientific discoveries and diverse application potentials. Ma and Sheng [112] discussed the development of acoustic metamaterials from the initial findings of mass density and bulk modulus frequency dispersions in locally resonant structures for acoustic wave band gap purposes. Zadpoor [46] presented an overview of mechanical metamaterials in which extremal materials such as pentamode, dilatational and auxetic metamaterials were discussed in the context of extremal properties of metamaterials.

#### 2.1.4. Pentamode materials

Extremal materials introduced by Milton and Cherkaev in 1995 [107], could behave extremely stiff in certain modes of deformation and extremely compliant in other modes. There are six eigenvalues in an elastic matrix defined in Eq. (1). If one eigenvalue of the metamaterial is very small and the others are large, then the material is referred to as the unimode material. If two, three, four, or five eigenvalues of the extremal material are very small, then the material is called bimode, trimode, quadramode, or pentamode material, respectively. Two specific categories of extremal materials, namely pentamode metamaterials, have received much attention in research community. Pentamode metamaterials with five very small eigenvalues are very compliant in five out of six deformation modes. This means a very large bulk modulus in comparison with the shear modulus. The very large bulk modulus indicates that the volume of pentamode metamaterials does not change with deformation. In other words, Poisson's ratio of the pentamode material approaches 0.5.

#### 2.1.5. Analogue to band gap

In order to engineer a phononic crystal in an acoustic atom scale, acoustic metamaterials with their inherent subwavelength nature have stimulated exciting investigations into band gap, negative bulk modulus and/or negative mass density. The metamaterials with periodic cellular structures can have an influence on the propagation of waves. When periodic cells are properly designed and arranged, elastic waves with frequency in a certain range can be blocked or significantly attenuated.

In general, materials with negative or extremal properties are unstable. Lakes and Wojciechowski [113] discussed the stability of metamaterials with negative compressibility and negative Poisson's ratio and observed negative bulk modulus in the pre-strained foam. They indicated that the constrained microscopic model exhibiting negative compressibility could be stable in structural analysis. Bunyan and Tawfick [114] discussed the structural stability of metamaterials with nonlinear stiffness and presented the designs to realize controlled essentially nonlinear response using the constrained elastic strut buckling. This indicates that the unit cell of extremal metamaterials needs to be properly constrained in practical application.

### 2.1.6. Nonlinear stress–strain and force–displacement relationships

As metamaterials consist of periodically arranged cellular structures or latticed elements, their relative densities are generally low and thus they are prone to large displacement, elastic buckling and plastic yielding. Therefore, geometrically nonlinear analysis is necessary, and materially nonlinear analysis is required for the plastic deformation.

Virk et al. [115] discussed energy dissipation via zero and negative stiffness of Kirigami cellular structures. The Kirigami (origami and cutting) cellular structures were produced in flat panels and curved configurations using a combination of rapid prototyping techniques and Kirigami procedures. The unusual stiffness features can lead to significantly increasing energy absorption during cyclic tests. Che et al. [116] proposed the use of small variations in the unit cell geometry to obtain a deterministic deformation sequence for one type of multi-stable metamaterial that consists of bi-stable unit cells, and presented an analytical model to analyze nonlinear mechanics. Luo and Tong [30] studied bi-stable and multi-stable cellular structural designs using topology optimization. Chronopoulos et al. [117] investigated the design of layered mechanical metamaterials with NS elements and their wave propagation properties. They showed that the layered metamaterial could exhibit superb acoustic insulation performance due to a large increase of the structural damping of the NS components.

Goldsberry and Haberman [118] designed the sub-wavelength structure of NS honeycombs allowed for direct control of the wave dispersion, which could be used as tuneable elastic metamaterials. This honeycomb structure was composed of a doubly periodic array of curved beams, and the nonlinear static elastic response due to large deformations of the NS unit cell could result in a large variation in linear elastic wave dispersion. Ha et al. [119] analyzed energy absorption via snap-through behaviors by designing an energy absorption lattice comprised of multiple tetra-beam-plate unit cells. Yu et al. [104] conducted a review on mechanical metamaterials associated with stiffness, rigidity and compressibility in which metamaterials were classified as lightweight, tuneable stiffness, negative compressibility ( $-4G/3 < K < 0$ ), pentamode ( $G \ll K$ ), and auxetic metamaterials ( $G \gg K$ ).

Nonlinear load–displacement relationships of metamaterials are essential to design vibration isolators with quasi-zero stiffness characteristics. As discussed above, metamaterials with peculiar properties can be efficiently used for vibration and sound mitigation. They may be classified into cellular structures with negative stiffness elements, auxetic, band gap and pentamode materials on the basis of their applications to vibration and sound control, which will be discussed in the following sections.

## 2.2. Cellular structures

As mentioned above, mechanical metamaterials are comprised of periodically arranged unit cells and the mechanical properties highly depend on the cell structures. The unit cell contains solid and void or fluid. The mechanical properties also rely on the relative density. For the specified relative density or the volume fraction, there exist theoretical bounds on elastic moduli of composites or cellular structures.

### 2.2.1. The Hashin-Shtrikman bounds

The Hashin-Shtrikman bounds are the tightest bounds of the possible range for composites with a two-phase material. The Hashin-Shtrikman bounds for bulk and shear moduli of the two phase composites are [120]:

$$K_1^* = K_1 + \frac{\nu_2}{\frac{1}{K_2 - K_1} + \frac{3\nu_2}{3K_1 + 4G_1}} \quad (10a)$$

$$K_2^* = K_2 + \frac{\nu_1}{\frac{1}{K_1 - K_2} + \frac{3\nu_1}{3K_2 + 4G_2}} \quad (10b)$$

and

$$G_1^* = G_1 + \frac{\nu_2}{\frac{1}{G_2 - G_1} + \frac{6(K_1 + 2G_1)\nu_1}{5G_1(3K_1 + 4G_1)}} \quad (11a)$$

$$G_2^* = G_2 + \frac{\nu_1}{\frac{1}{G_1 - G_2} + \frac{6(K_2 + 2G_2)\nu_2}{5G_2(3K_2 + 4G_2)}} \quad (11b)$$

where  $\nu_1$  and  $\nu_2$  represent the volume fractions of materials 1 and 2,  $K_1^*$  and  $K_2^*$  denote the lower and upper bounds of the effective bulk moduli when  $K_2 > K_1$ ,  $G_1^*$  and  $G_2^*$  are the lower and upper bounds of the effective shear moduli when  $G_2 > G_1$ .

For a two-dimensional isotropic cellular structure consisting of a solid with volume fraction  $\nu$  and a void with volume fraction  $(1 - \nu)$ , the Hashin-Shtrikman upper bounds of the effective moduli are given by [120,121]:

$$\frac{K_e}{K} \leq \frac{G\rho_e}{K(1 - \rho_e) + G} \quad (12a)$$

$$\frac{G_e}{G} \leq \frac{K\rho_e}{(K + 2G)(1 - \rho_e) + K} \quad (12b)$$

where  $\rho_e$  is the relative density of the cellular structure ( $\rho_e = \nu$ ),  $K_e$  and  $G_e$  represent the effective bulk modulus and shear modulus, respectively.

In the low-density material ( $\nu \rightarrow 0$ ), the Hashin-Shtrikman upper bounds become:

$$\frac{K_e}{K} \leq \frac{G\rho_e}{K + G} \quad (13a)$$

$$\frac{G_e}{G} \leq \frac{K\rho_e}{2(K + G)} \quad (13b)$$

For the high density limit ( $\nu \rightarrow 1$ ), the bounds are given by:

$$\frac{K_e}{K} \leq 1 - \frac{(K + G)}{G}(1 - \rho_e) \quad (14a)$$

$$\frac{G_e}{G} \leq 1 - 2 \frac{(K + G)}{K}(1 - \rho_e) \quad (14b)$$

Two-dimensional isotropic cellular structures must obey the above bounds. Berger et al. [122] showed that mechanical metamaterials could achieve the theoretical limit of isotropic elastic stiffness or the Hashin-Shtrikman upper bounds. Fig. 5 illustrates the Hashin-Shtrikman bounds of bulk and shear moduli of cellular structures, in which  $\nu$  is the volume fraction or the relative density,  $K_e$  and  $G_e$  are the effective bulk modulus and shear modulus [121]. The effective moduli for the optimized triangular, kagome and hexagonal cellular structures are also indicated.

### 2.2.2. Cellular structures

Materials with cellular structures widespread in nature can exhibit peculiar mechanical properties and some examples are given in Fig. 6. These cellular materials have evolved over thousands of years so that they have been progressed to an optimal architecture and may span over multiple hierarchies across different length scales. For instance, the highly complex porous architecture of a bone core consisting of intricately-shaped ligaments and density gradients allows it to achieve a much higher structural efficiency as compared to the synthetized cellular materials by human. Natural tubular structures

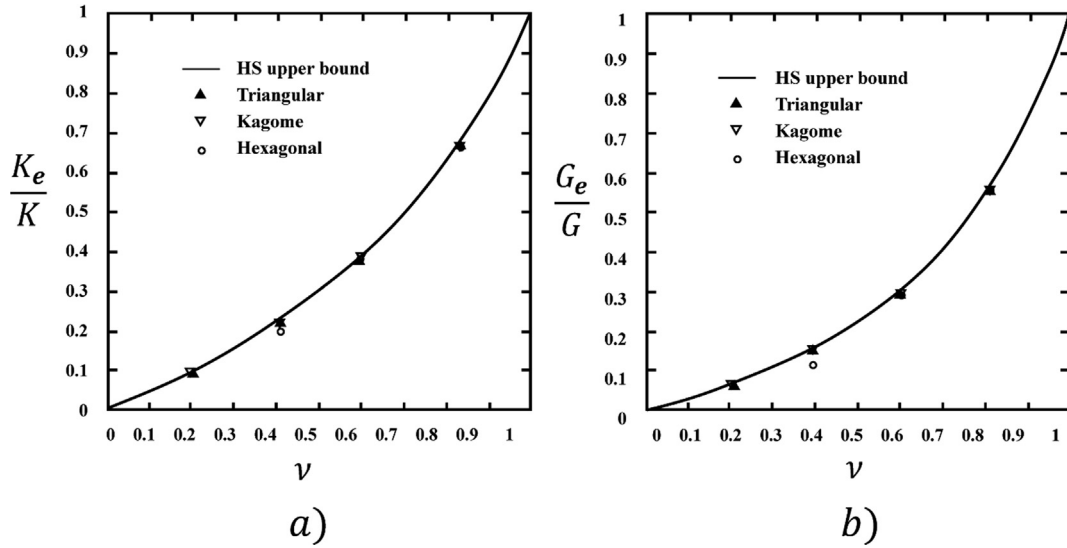


**Fig. 5.** The Hashin-Shtrikman upper bounds of bulk modulus and shear modulus: (a) non-dimensional effective bulk modulus  $K_e/K$  versus volume fraction, and (b) non-dimensional effective shear modulus  $G_e/G$  versus volume fraction.

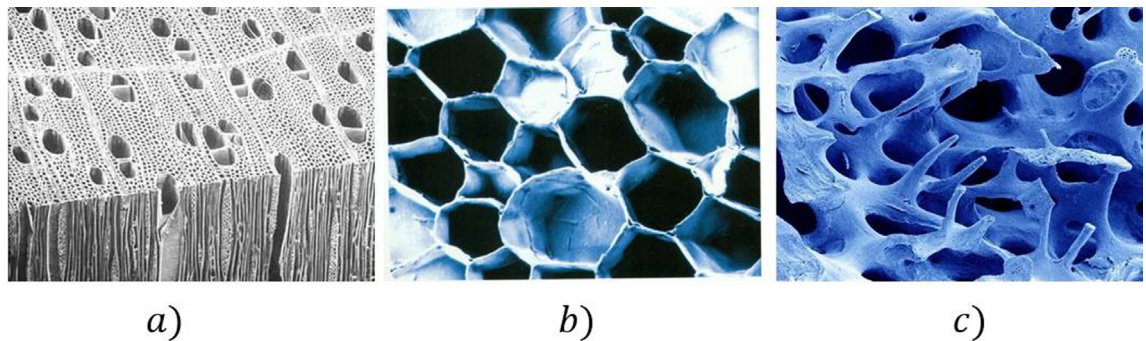


**Fig. 6.** Cellular structures found in nature: (a) bole fiber, (b) cork, and (c) trabecular bone.

often have a honeycomb-like or foam-like core supporting a denser outer cylindrical shell and they have high resistance of the shell to kinking or local buckling failure.

Bio-inspired by various biomaterials in nature, engineered cellular structures have been investigated by many researchers. Luo and Tong [123,124] designed and tested adaptive pressurized cellular structures for shape morphing. Gramüller et al. [49] presented a concept of biologically inspired pressure actuated cellular structures. Lv et al. [125] studied an efficient design method for plant bio-inspired fluidic cellular structures composed of polygonal motor cells using topology optimization. Tancogne-Dejean et al. [126] designed plate-lattices by placing plates along the closest-packed planes of crystal structures and discussed their applications for heat-exchange, thermal insulation, acoustics, and biomedical engineering. Alfouneh et al. [127] designed multi-cellular cores for sandwich panels by topology optimization to attenuate harmonic excitations.

Cellular structures are typically classified into bending and stretching dominated structures in terms of deformation, as shown in Fig. 7 [48]. Due to the effective energy absorption ability of the cellular structures, they have been used in engineering for vibration attenuation and sound absorption.

For a typical cellular structure, stress-strain curves under compression shown in Fig. 8 may be characterized by three regimes [128]: 1) a linear elastic regime with cell edge bending or face stretching; 2) a stress plateau associated with progressive cell collapse by elastic buckling, plastic yielding or brittle crushing, depending on the mechanical properties of the base materials; and 3) densification, corresponding to the collapse of the cells throughout the material and subsequent loading of the cell edges and faces against one another. Cellular materials normally have low relative densities of 10–20% so that they can be deformed up to large strains of 70–80% before densification occurs. In tension, the linear elastic response is the same as in compression. As the strain increases, the cells become more oriented with the loading direction, increasing the stiffness of the material until tensile failure occurs.

Cellular structures have become available with the aid of recent developments in advanced manufacturing technologies. The 3D printing technology enables fabrication of cellular materials with complex architectures across several length scales, with feature sizes down to the nanometer scale for a wide range of materials [129,130]. Bückmann et al. [53] studied 3D mechanical metamaterials with positive, zero and negative Poisson's ratios and with sufficient overall size for direct mechanical characterization made by dip-in direct-laser-writing optical lithography. Schaedler and Carter [45] reviewed architected cellular materials fabricated by additive manufacturing and progression in 3D printing techniques for micro-

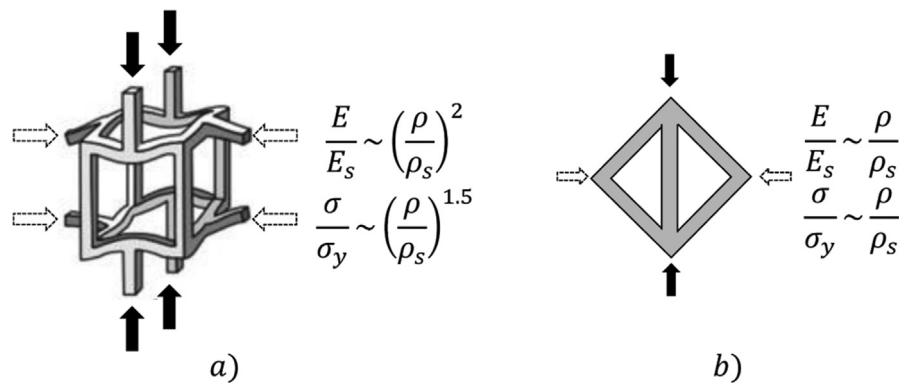


**Fig. 7.** Bending and stretching dominated behaviors in cellular materials: (a) influence of relative density on the mechanical properties of a bending cellular structure, and (b) relative density of a stretching-dominated cellular architecture.

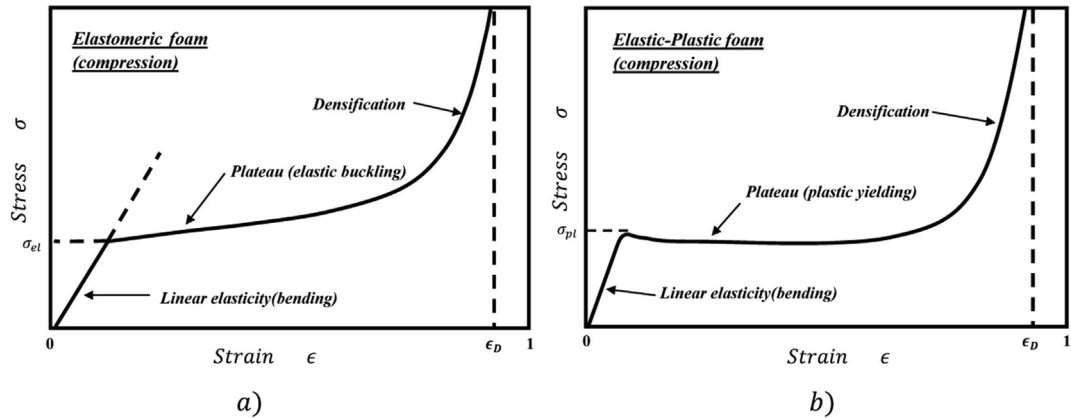


**Fig. 8.** Schematic uniaxial stress–strain curves for: (a) elastomeric foam in compression, (b) elastic–plastic foam in compression.

lattices with graded porosity and truss structures. Li et al. [131] presented a design of mechanical metamaterials with both mechanical wave filtering and energy harvesting functions.

### 2.2.3. Nonlinear property for vibration isolation

A complete band gap can be created via the coupling of the bulk elastic wave propagating along the structural frame and the distributed local resonance associated with the square array of piezoelectric cantilevers. Debeau et al. [132] fabricated fully recoverable negative stiffness honeycombs from thermoplastic and metallic materials. The fabricated metamaterials with negative stiffness honeycombs utilized elastic buckling to absorb mechanical energy and offered some advantages, such as the ability to recover their initial configuration and repeatable mechanical energy absorption. Sridhar et al. [133] demonstrated that micro-inertial continuum based local resonance metamaterials exhibited sub-wavelength negative stiffness effects. Bonatti and Mohr [134] studied the mechanical behaviors of additively-manufactured anisotropic and isotropic smooth shell-lattice materials and showed their exceptional specific energy absorption capacity.

Periodic elastic lattice materials are a type of cellular materials with unique properties that cannot be achieved by the fully uniform solids. Cohen et al. [135] discussed modeling for the non-linear elastic response of periodic lattice materials based on a representative volume element comprised of one or more unit cells. Typical compressive stress–strain curves of an elastomeric foam and elastic–plastic foam shown in Fig. 8 indicate that cellular structures are efficient in energy absorption for vibration mitigation and even can realize quasi-zero stiffness for effective vibration isolation.

## 2.3. Auxetic metamaterials

Auxetic metamaterials are known as cellular structures with designed unit cells and can have unique characteristics such as negative Poisson's ratio, large damping factor, high energy absorption and dissipation.

### 2.3.1. Poisson's ratio

Poisson's ratio is defined as a ratio of transverse strain to longitudinal strain with respect to force applying direction. When tensile deformation is considered as positive and compressive deformation as negative, the definition of Poisson's ratio contains a minus sign and thus normal materials have a positive Poisson's ratio. As the thermodynamically permitted range of Poisson's ratio in isotropic materials is  $-1 < \nu < 0.5$ , the possibility of a negative Poisson's ratio has been proposed for a long time based on the classical elasticity theory.

In early stage, negative values were known in some directions in single crystals but unknown in isotropic materials. Robert [136] studied negative Poisson's ratio structures, such as 2D inverted honeycombs and hinged structures of rods. Lakes [137] produced an open-cell cellular solid with the negative Poisson's ratio by using a commercial reticulated foam as precursor. The term auxetic was introduced in [138] that proposed a molecular structure based on negative Poisson's ratio honeycomb and the term has then been widely used for simplifying the long phrase. The material with negative Poisson's ratio has also been termed as the dilatational material as it can easily change in volume but is difficult to shear [106].

A distinctive feature of the auxetic material is the higher resistance to shear strain and thus to resist shear stress waves. Poisson's ratio influences wave speeds. If Poisson's ratio is large, longitudinal waves propagate much faster than shear waves. On the other hand, if it is sufficiently small, shear waves propagate faster than longitudinal waves. Shear resistance is particularly important in structural components such as sheets or beams in buildings, automotive vehicles and aircrafts.

Bulk and shear moduli are mainly resistant to volumetric and shape deformations, respectively. Relationships of  $E$ ,  $G$ ,  $K$  and  $\nu$  are given in Eqs. (7)–(9). In conventional isotropic materials,  $0 < \nu < 0.5$ , and thus Young's modulus is at least twice the shear modulus on the basis of Eq. (7). However, when  $-0.5 < \nu < 0$ , the Young's modulus  $E$  is in the range of  $G$  to  $2G$ , and

the two moduli are equal at  $\nu = -0.5$ . This means that the material is easy to compress but difficult to shear. When  $-1 < \nu < -0.5$ , the shear modulus exceeds Young's modulus and when  $\nu \rightarrow -1$ ,  $G \gg K$  in light of Eq. (9), then the material will be difficult to shear but easy to deform volumetrically.

When a conventional material is subjected to impact loading, the force compresses the material. Nevertheless, when an object impacts onto an auxetic metamaterial and compresses it in loading direction, the auxetic material also contracts laterally. This creates an area of denser material, which will resist indentation as shown in Fig. 9 [139]. The negative Poisson's ratio foam shows an overall superiority of damping and acoustic properties in comparison with the conventional foam [139]. Auxetic foams have better sound absorption and energy dissipation capacities than the conventional foams in most ranges of frequencies. Therefore, an auxetic metamaterial can effectively refract or dissipate stress waves.

Prawoto [140] reviewed auxetic materials focusing on computations and mechanics. Babaee et al. [54] explored buckling deformations to design 3D metamaterials with negative Poisson's ratios. Hewage et al. [141] showed that a composite material or structure might display a simultaneous reversal in directions of deformations for the axial and transverse dimensions, corresponding to negative values of effective stiffness and effective Poisson's ratio, respectively. Huang and Chen [142] reviewed progress in functional materials with a negative Poisson's ratio and discussed the coexistence and correlations of the negative Poisson's ratio with other negative indexes such as the compressibility and the thermal expansion.

### 2.3.2. Re-entrant honeycomb metamaterials

Honeycomb structures have been widely used in lightweight sandwich panels and cellular structures to absorb impact energy and attenuate structural vibration. Auxetic honeycomb structures are attractive for various engineering applications due to their volume change control capacities and excellent impact energy absorption performance. Yang et al. [143] established an analytical model of a 3D re-entrant honeycomb structure based on a large deflection beam model. Analytical solutions for the modulus, Poisson's ratio and yield strength of the cellular structure in principal directions were obtained and compared with the experimental results and finite element analysis. Fig. 10 shows a regular honeycomb with positive Poisson's ratio and a re-entrant honeycomb with negative Poisson's ratio.

Li et al. [144] built a series of 2D random cellular solid models with re-entrant structures in light of a modified Voronoi tessellation technique. Poisson's ratio and energy absorption capacity of cellular solid models with different initial relative densities were studied and the minimum Poisson's ratio of  $-0.38$  was obtained. They showed that the cellular structures with minimum negative Poisson's ratio could have the highest energy absorption capacity in this series of designs. Fu et al. [145] proposed a novel design of honeycomb by embedding the rhombic configuration into the normal re-entrant honeycomb structure to improve its in-plane mechanical properties. They found that this design of honeycomb could maintain auxetic performance, while both the in-plane Young's modulus and the critical buckling strength were considerably enhanced as compared to the normal re-entrant hexagonal honeycomb. Ingole et al. [146] presented the design of auxetic-strut structures, and showed that the locally reinforced auxetic-strut structure with lower values of Poisson's ratio could absorb more energy than other related structures.

The recent advance in additive manufacturing techniques has enabled fabrication of materials with arbitrarily complex micro- and nano-architectures to form mechanical metamaterials. Kolken and Zadpoor [147] studied the topology-property relationship in three types of auxetic metamaterials, namely re-entrant, chiral, and rotating (semi-) rigid structures. Lakes [148] studied metamaterials with negative Poisson's ratio governed by the geometry of interatomic bonds and investigated the role of Poisson's ratio in 2D and 3D metamaterials and phase transformations. Dudek et al. [149] discussed the concept of allowing the control of the stiffness of a particular class of re-entrant auxetic magneto-mechanical metamaterials through the introduction of magnets to the system and showed that the appropriate insertion of magnets in such a system would alter its stiffness, and even making it exhibit negative stiffness and negative Poisson's ratio at the same time. Such

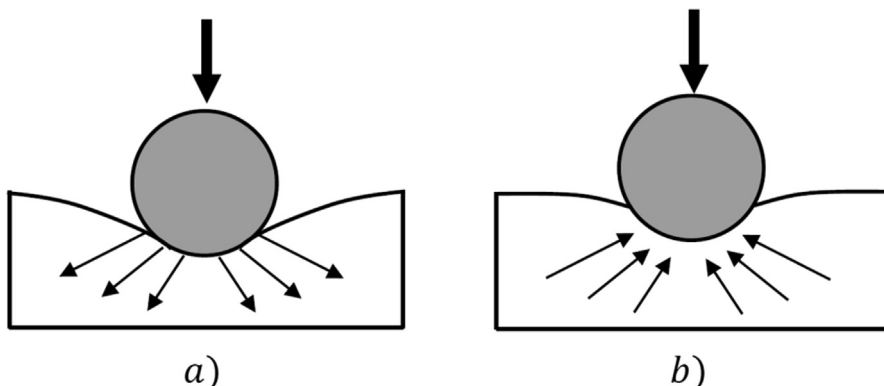


**Fig. 9.** Impact/indentation performance: (a) conventional material, and (b) auxetic material.

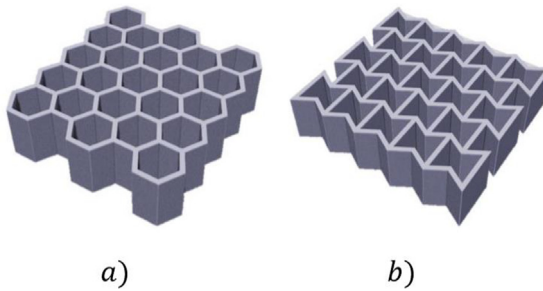


**Fig. 10.** Honeycomb: (a) regular hexagons, and (b) inverted hexagons or re-entrant honeycomb.

systems have the potential to be used in a wide range of practical applications such as damping vibration in which NS components are fundamentally important.

### 2.3.3. Auxetic property, damping, energy absorption and dissipation

Auxetic materials have better indentation resistance, impact shielding capability and enhanced toughness as shown in Fig. 9. Li et al. [150] reported a class of high-performance composites in which auxetic lattice structures were used as the reinforcements and the nearly incompressible soft material was employed as the matrix. Experimental and FEA results showed that the compressive behavior of this type of the auxetics reinforced composites that were fabricated by the 3D printing technique achieved a significant enhancement of stiffness and energy absorption. Ren et al. [47] presented a review on auxetic metamaterials and fabrication methods to generate 3D metallic auxetic metamaterials.

Based on the property of auxetic materials, Ren et al. [151] designed nails with the auxetic property for easier push-in and harder pull-out, and they further [152] studied a simple geometrical shape to achieve 3D auxetic behaviors. Chen et al. [153] investigated vibration damping mechanisms of composite 3D double-arrow-head auxetic metamaterials which were made from carbon fiber reinforced polymer using an assembly method. The damping performance of this structure was characterized by compressive loading-unloading and sine sweep frequency tests. The results showed that the structure consumed more energy with an increase of the strain level. The contribution of macroscopic frictional energy and elastic buckling energy consumption was much greater than that of intrinsic material in energy dissipation.

Auxetic materials become thicker rather than thinner when they are stretched. This property is well suitable to design shape transforming metamaterials. Nevertheless, current auxetic designs are often mono-stable and cannot retain the transformed shape after load removal. Inspired by ancient geometric motifs arranged in square and triangular grids, Rafsanjani and Pasini [154] proposed a class of switchable architected materials that could exhibit auxeticity and structural bi-stability simultaneously. The material concept was experimentally realized by perforating various cut motifs into a sheet of rubber to generate a network of rotating units connected with compliant hinges. By making use of the auxetic property, mechanical properties such as fracture toughness and indentation resistance, can be considerably improved. Saxena et al. [55] reviewed auxetic materials and showed their excellent behaviors in energy absorption and dissipation.

Qin and Yang [155] proposed a topology optimization design method for metamaterials to mitigate structural vibration. The metamaterials were generated by periodically arranging the unit cells to generate auxetic property. Numerical simulations showed that the amplitudes of the acceleration response could be reduced by 66.5% after passing through the metamaterials. The functional element based metamaterials could achieve more than 12% improvement in vibration mitigation as compared to the conventional honeycomb materials.

Inspired by non-uniform or nonhomogeneous metamaterials, Li and Yang [156] studied annular cellular structures composed of auxetic metamaterials with graded negative Poisson's ratios. The static stiffness and vibration-acoustic performance of two types of structures were explored and compared to show the advantages in vibration and sound reduction applications.

As illustrated in Fig. 9, auxetic metamaterials can dissipate impact or shock energy via transverse deformation due to the negative Poisson's ratio property and thus they can be fabricated as protective structures against dynamic loading. Typical stress-strain curves of re-entrant cellular structures are similar to those of the conventional cellular structures as illustrated in Fig. 8. The curves include an elastic region, plateau and final densification. In addition, the curves can fluctuate due to snap-through behaviours and the plateau region can be much wider than that of the conventional cellular structure and thus the re-entrant cellular structures have high energy absorption capacity. Accordingly, auxetic metamaterials can be efficiently used for vibration control.

### 2.4. Band gap metamaterials

The band gap property of acoustic metamaterials can be used for controlling propagation of stress waves. In the band gap metamaterials, stress waves with a specific range of frequencies cannot propagate through or can be considerably reduced.

Acoustic metamaterials with the low-frequency band gaps are particularly useful for practical engineering applications such as vibration control, sound mitigation and insulation in the low frequency band.

#### 2.4.1. Approaches of band gap metamaterials to attenuate wave propagation

When wave propagation depends on periodic arrangement of scatterers inside the medium, the scatterers are referred to as phononic crystals. In phononic crystals, one of the most important features is the effect of Bragg gaps that were induced by destructive interference of waves scattered from inclusions [157]. As a result, waves with a certain range of frequencies may not be propagated. Based on a concept of localized resonant structures, Liu et al. [38] fabricated sonic crystals that could exhibit spectral gaps with a lattice constant which is two orders of magnitude smaller than the relevant wavelength. Ruzzene et al. [158] analysed the wave effects in two dimensional cellular structures and showed the phase constant surfaces defining the directions of waves propagating in the plane of the structure for the prescribed frequency range. Generally, bandgap phenomena in mechanical metamaterials or phononic crystals can be achieved by the artificial unit cells which prevent wave propagation with internal resonance origination from internal resonator or Bragg scattering generated from periodicity.

Vibration suppression could be achieved by designing hierarchical metamaterials using light-weight structures and materials [159]. Dynamical properties of periodic structures were specifically studied for their band gap characteristics, which enables the design of structures to block stress waves with a certain range of frequencies [160]. Bandgap phenomena in elastic metamaterials or phononic crystals could be obtained by the artificial unit cells which prevent wave propagation with Bragg scattering or internal resonance [161]. Metamaterial-based elastic wave absorbers were actually based on a concept of conventional mechanical vibration absorbers, which utilized the local resonance of subsystems to generate inertia forces to work against the external load and prevented elastic waves from propagating forward [51].

Various strategies have been proposed in the field of mechanical metamaterials to widen band gaps for vibration suppression by Bragg scattering and/or local resonant effects. Fig. 11(a) and 11(b) illustrate dispersion curves of metamaterials based on Bragg scattering and local resonant effects, where  $\omega$  and  $\kappa$  denote the frequency and the wave number [149].

#### 2.4.2. Locally resonant sub-structures

A periodic chain shown in Fig. 12(a) has been widely used as a local resonant model to study wave propagation in periodic materials with the damping effects neglected [161–163].

The equation of motion of the  $n^{\text{th}}$  unit cell can be written as [63,108,161]:

$$m\ddot{u}_n + k_s(2u_n - u_{n-1} - u_{n+1}) = 0 \quad (15)$$

where  $u_n$  is the displacement of the  $n^{\text{th}}$  unit cell,  $m$  and  $k_s$  denote the mass and stiffness.

The wave solution can be assumed as:

$$u_n = \frac{A_n}{2} e^{i(\kappa dn - \omega t)} + \frac{\bar{A}_n}{2} e^{-i(\kappa dn - \omega t)} \quad (16)$$

where  $\omega$ ,  $\kappa$ , and  $A_n$  are the frequency, wave number and amplitude.

Considering the real value,  $A_n = \bar{A}_n$ , and substituting Eq. (16) into Eq. (15) yields:

$$-m\omega^2 + 2k_s(1 - \cos\kappa d) = 0 \quad (17)$$

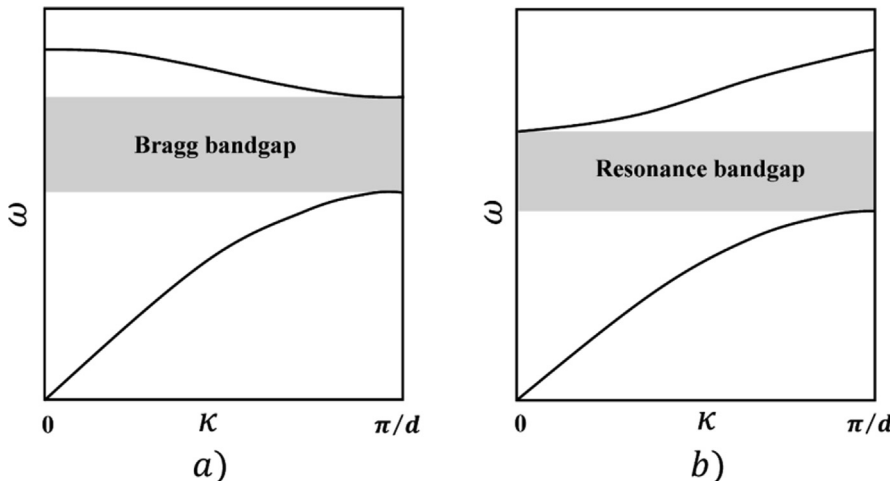


**Fig. 11.** Schematic dispersion curves: (a) Bragg bandgap, and (b) internal resonance bandgap.

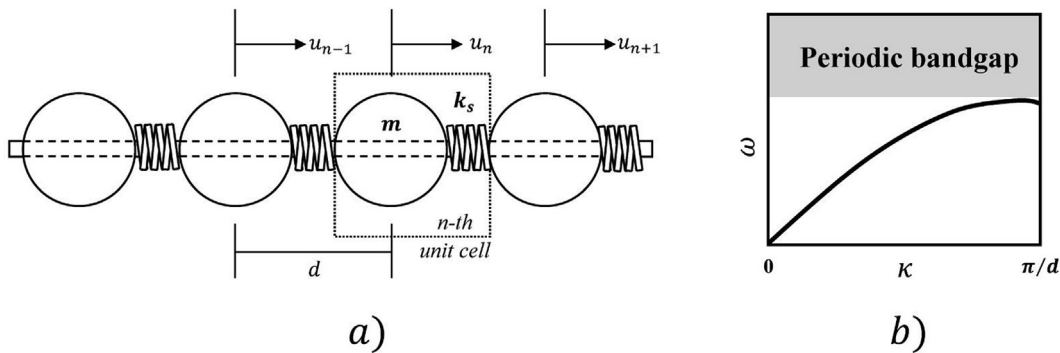


**Fig. 12.** A local resonant model for periodic metamaterials: (a) periodic mass-spring chain, and (b) dispersion curve.

Then the wave dispersion equation is obtained as:

$$\bar{\omega}^2 = \frac{\omega^2}{(k_s/m)} = 2(1 - \cos\kappa d) \quad (18)$$

where  $\kappa d$  represents a complex dimensionless wavenumber.

Fig. 12(b) shows a typical dispersion curve of the periodic resonant chain in linear analysis for the system in the absence of damping. Eq. (18) illustrates that if the value of  $\cos(\kappa d)$  is not in the range of  $[-1, 1]$ ,  $\kappa$  becomes a complex number, indicating that a band gap is formed. Therefore, the band gap condition for the linear periodic chain is given by:

Pass band if:  $0 \leq \bar{\omega}^2 \leq 4$  (19a)

Stop band if:  $4 < \overline{\omega}^2$  (19b)

If the masses are connected with nonlinear springs in Fig. 12(a), the force–displacement relationship may be defined as:

$$F = k_s x + k_h x^3 \quad (20)$$

where  $k_n$  is the nonlinear stiffness.

The equation of motion can be expressed as:

$$m\ddot{u}_n + k_s(2u_n - u_{n-1} - u_{n+1}) + \varepsilon k_n(u_n - u_{n-1})^3 + \varepsilon k_n(u_n - u_{n+1})^3 = 0 \quad (21)$$

where  $\varepsilon$  is the small perturbation parameter.

The nonlinear dispersion equation can be derived as [161,164]:

$$\overline{\omega} = \overline{\omega}_0 + \varepsilon \frac{3\bar{k}_n A_n^2 \overline{\omega}_0^3}{8} + O(\varepsilon^2) \quad (22)$$

where

$$\bar{k}_n = \frac{k_n}{k_s}, \quad \bar{\omega}_0^2 = \frac{-2 \pm 2\sqrt{1 + 3\varepsilon\bar{k}_n A_n^2 \bar{\omega}^2}}{3\varepsilon\bar{k}_n A_n^2}$$

To investigate the band gap condition for the nonlinear periodic chain, both sides of Eq. (22) are squared as [161,164]:

$$\bar{\omega}^2 = \bar{\omega}_0^2 + \varepsilon \frac{3\bar{k}_n A_n^2 \bar{\omega}_0^4}{4} + O(\varepsilon^2) \quad (23)$$

The band gap conditions are given by:

The band gap  
Pass band if:

$$0 < \overline{\omega}^2 < 4 + 12\epsilon k_1 A_2^2 \quad (24a)$$

Stop band if:

$$4 + 12\varepsilon k_* A_2^2 < \overline{\omega}^2 \quad (24b)$$

In addition to the band gaps governed by Bragg scattering and local resonance, Bae and Oh [161] reported another type of bandgap phenomenon referred to as amplitude-induced bandgap that was caused by the amplitude in nonlinear metamaterials.

Gantzounis et al. [165] addressed the formation of low-frequency band gaps in locally resonant granular crystals in which the discrete equations of motion were used to study dynamics of the metamaterials. They also investigated quasi-linear

behaviours and showed that the stop band could be introduced at about one octave lower frequency than in materials without local resonances. By strategically tailoring the non-uniform local resonance parameters, broadband and multi-frequency stop band characteristics could be obtained. Chang et al. [166] discussed wave propagation behaviours and attenuation mechanism of the elastic metamaterial with locally resonant sub-structures, in which the wave attenuation mechanism and the dynamic responses of metamaterials were analysed from the energy point of view. They found that the coupled Bragg-resonance band gap was much wider than the locally resonant band gap. Xu et al. [159] proposed metamaterials with hierarchically arranged local resonators that possessed the ability to efficiently tailor elastic wave or vibration attenuation to various frequency ranges via different hierarchical designs. A honeycomb hierarchical lattice with embedded rubber-coated lead cylinders was designed to demonstrate the vibration suppression at subwavelength scales in two separate frequency ranges. The hierarchical metamaterials could benefit low-frequency passive vibration isolation and stress wave mitigation by using light-weight structures.

#### 2.4.3. Linear band gap acoustic metamaterials and applications

Zhu et al. [167] studied mechanical metamaterials with chiral microstructure made of a single-phase solid material to achieve negative refraction of elastic waves. They [168] further investigated an elastic metamaterial beam with the chiral microstructure for broadband vibration suppression. In this investigation, a theoretical beam model with multiple resonators was developed to investigate band gap behaviours of the elastic metamaterial beam and an elastic metamaterial beam with section-distributed resonators was considered to enable broadband vibration mitigation. Han et al. [169] designed a type of cellular materials named the shellular whose cells were composed of a continuous, smooth-curved shell in light of the minimal surface theory for band gap vibration attenuation.

Matlack et al. [170] studied phononic crystals and acoustic metamaterials with the band-gap property to prevent certain frequencies from propagating through metamaterials, with potential applications into the control of structural vibration and noise. Wang et al. [171] proposed a tuneable digital metamaterial consisting of primary lattices and auxiliary beams with electromagnets, in which the beams with the electromagnets in the unit cell formed an auxiliary structure to attach to the cell frame. The designed metamaterials behaved as a local resonator to attenuate elastic wave propagation with a frequency range of 5.5–7.5 Hz. Messner [172] presented a method for optimizing the mesostructure of lattice-structured materials, formed by periodic arrays of slender members resembling lightweight macroscale structures.

Sugino et al. [173] studied the mechanism of bandgap formation in locally resonant mechanical metamaterials. To effectively utilize such locally resonant metamaterial concepts in finite structures, it was required to bridge a gap between the lattice dispersion characteristics and modal behaviour of the host structure with the resonators. This theoretical framework was verified by experiment using a locally resonant cantilever beam under bending vibration. Harne and Urbanek [174] used local buckling modes in constrained metamaterials to enhance broadband vibration energy suppression. They introduced an elastomeric metamaterial, ideal for embedding into a practical engineering structure for vibration control. They found that triggering local buckling deformations could provide a valuable balance between stiffness reduction and dynamic mass, leading to magnifying the effective damping effects.

As shown in Fig. 12, a metamaterial-based elastic wave absorber can be a uniform isotropic bar with a series of small spring-mass subsystems attached at the divided longitudinal locations to form the band gap. The stop band does not allow waves to propagate further. Pai [51] presented modelling and analysis for band gap metamaterials and revealed the working mechanism of longitudinal metamaterial bars in the elastic wave absorption capacity. Xiang et al. [175] experimentally validated a kind of layered periodic foundation with concrete and rubber layers for frequency band gap applications. When the frequency of an elastic wave falls in a range of band gap frequencies, the wave and its energy can be attenuated or the wave cannot travel through the foundation so that the foundation itself can serve as a vibration isolator.

Al Ba'ba'a et al. [176] used transfer functions to understand the formation of band gaps in locally resonant mechanical metamaterials, and derived a closed form expression for the transfer function by identifying a recursive approach for serially arranged locally resonant mass in mass cells. The developed transfer function approach for computing and evaluating band gaps in locally resonant structures provided a framework for manipulation of control techniques to modify and to tune band gaps in finite acoustic metamaterials. Krushynska et al. [177] proposed a single-phase solid metamaterial with quasi-resonant Bragg band gaps and studied the coupling effects of local resonators with Bragg band gaps in single-phase mechanical metamaterials.

Brûlé et al. [178] experimentally studied seismic metamaterials by measuring the velocities of particles and the seismic energy distribution, showing the importance of metamaterials in civil engineering applications. Chen et al. [179] presented active elastic metamaterials containing negative capacitance piezoelectric shunting. They investigated dispersion curves and band gap control of an active mass-in-mass lattice system, and showed that the band gaps can be actively controlled and tuned by properly selecting the value of negative capacitance of piezoelectric ceramics. Li et al. [131] demonstrated simultaneous mechanical wave filtering and energy harvesting using piezoelectric metamaterials that are composed of a square array of free-standing cantilevers attached to a primary structural frame, to achieve vibration isolation and energy harvesting.

#### 2.4.4. Nonlinear band gap metamaterials

Huang and Sun [63] studied wave attenuation mechanism in an acoustic metamaterial with negative effective mass density. The attenuation of wave amplitude for frequencies in the stop band was studied from the energy transfer point of view. It was found that most of the work done by the external force was stored in the internal mass if the frequency of the external force was close to the locally resonant frequency. Huang and Sun [50] further investigated dispersion curves and the band

gap structure of a multi-resonator mass-in-mass lattice system by considering the unit cell of the lattice system consisting of the separate masses connected by linear springs. Naify et al. [180] showed that acoustic metamaterials with negative dynamic mass density could significantly increase the transmission loss over mass law predictions for a band gap with frequency of 100 Hz.

Nonlinearity and dissipation are two important aspects of mechanical metamaterials for propagation of stress waves. Fang et al. [181] theoretically and experimentally studied the nonlinear chaotic mechanism in 1D and 2D nonlinear acoustic metamaterials and showed that this mechanism enabled nonlinear acoustic metamaterials to reduce wave transmissions by as much as 20–40 dB in an ultra-low and ultra-broad band. Jiang and He [182] reported a dual-directionally tuneable acoustic metamaterial comprised of a matrix and two spiral beams with an embedded permanent magnet. Two types of vibration modes with band gaps were observed under out-of-plane and in-plane excitations. The out-of-plane and in-plane transmissions of the metamaterial could move toward two directions due to their modal characteristics when external magnets were introduced to tune the magnetic force monotonically, which provided application potentials for low-frequency vibration isolation in practical environments.

Reynolds and Daley [52] studied a type of active viscoelastic metamaterial with double negativities, which could significantly attenuate elastic waves over wide frequency bands. Xu et al. [183] presented a nonlinear dissipative elastic metamaterial in a triatomic mass-spring chain to explore the interplay between nonlinearity and dissipation for broadband wave attenuation. Krushynska et al. [184] investigated a class of lightweight metamaterials with accordion-like *meta*-structures capable of strongly attenuating low-frequency elastic waves through numerical simulations.

Inspired by the hierarchical structures of butterfly wing surfaces, Wu et al. [185] proposed lattice structures with two-order hierarchically-periodic architectures and investigated their band-gap characteristics using a spectral element method. D'Alessandro et al. [160] presented ultra-wide 3D band gap metamaterials with extremely low frequency band of operation. Wang et al. [186] proposed a local resonant rod with high-static-low-dynamic-stiffness resonators to create a low-frequency band gap for longitudinal wave propagation by using NS mechanism. Nonlinear quasi-zero-stiffness (QZS) metamaterials have been found effective to isolate vibration. Wu et al. [187] designed an elastic metamaterial beam containing X-shaped local resonators for vibration attenuation. Cai et al. [188] proposed 1D QZS metamaterials to acquire very low-frequency band gaps and used a lumped-mass-spring chain model to reveal the dispersion relations and the band gaps.

Meza et al. [129] studied hierarchical structures spanning across multiple length scales in natural biomaterials like glass sponge skeletons and manmade structures like Eiffel Tower. Although mechanical robustness and damage tolerance hierarchical structures stemming from sophisticated ordering within the constituents have been extensively studied, the specific role of hierarchy remains to be fully understood and the capability of energy shielding in a range of frequency band has yet been achieved. Wu et al. [189] presented a mechanical metamaterial for energy shielding by circulating energy between a metamaterial and an energy source. The energy shielding effects were experimentally demonstrated in ultralow frequency ranges. Along with the energy bypass and energy absorption mechanisms, the energy shielding metamaterials could provide design options for metamaterials with unprecedented dynamic characteristics at different length scales.

As discussed above, metamaterials with band gap characteristics are promising solutions for wave control and vibration mitigation in various frequency ranges. Despite recent advances in the design of phononic crystals and acoustic metamaterials, generating wide band gaps in low frequency ranges in practically feasible metamaterials remains a great challenge. The motion equation of the nonlinear band gap metamaterial can be described by Eq. (21). Nevertheless, how to design linear and nonlinear spring components shown in Eq. (20) remains open.

## 2.5. Pentamode metamaterials

Pentamode metamaterials are artificial solids with elastic properties similar to those of liquids. Milton and Cherkaev [107] showed that all conceivable mechanical materials could be synthesized based on pentamode materials.

### 2.5.1. Structures of pentamode materials

Since the elastic matrix  $C$  defined in Eq. (1) is symmetrically-positive definite, it can be diagonalized by the orthogonal transformation. After this transformation, six positive eigenvalues are obtained and the corresponding eigenvectors are associated with the material deformations. A small eigenvalue represents the strain associated with the easy mode of deformation and if an eigenvalue equals to zero, it represents a floppy mode. In a two-dimensional (2D) problem, there are three eigenvalues. If all the three eigenvalues of a material are large, it is referred to as a nullmode material and thus there are no easy deformation modes. If two eigenvalues are large and one eigenvalue is very small, it is called a unimode material because there is one easy deformation mode. A material with Poisson's ratio being close to  $-1$  is an example of an extremal unimode material in which one eigenvalue is close to 0. A simple laminate of the two phases is an example of a bimode material, in which there are two easy modes of deformations, as shown in Fig. 13(a). A pentamode material in three-dimensional analysis is the material with five easy deformation modes; that is, five out of six eigenvalues are very small and one is large. The pentamode structure proposed in [107] and discussed in [190] is schematically shown in Fig. 13(b).

### 2.5.2. Property of pentamode metamaterials

As discussed above, pentamode metamaterials are artificial solids with properties approximate to those of liquids. When Poisson's ratio of the material approaches 0.5, the materials will act as liquid as shown in the Milton map of Fig. 2. On the

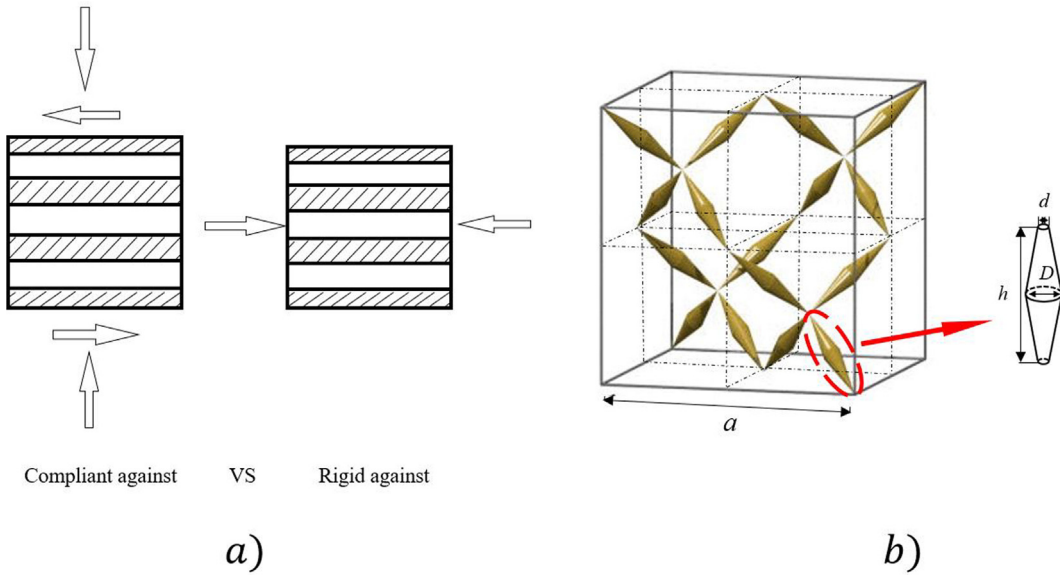


**Fig. 13.** Examples of (a) the two-phase bimode material, and (b) artificial diamond symmetric crystal (pentamode metamaterial with approximation of the stable microstructure).

basis of Eq. (9), when Poisson's ratio approaches 0.5,  $(K/G) \rightarrow \infty$ ; that is, shear modulus would approach zero or bulk modulus would approach infinity. The infinitive bulk modulus makes it incompressible and the near zero shear modulus means that ideal pentamode metamaterials would immediately flow away when they are subjected to shear stress. Accordingly, the mechanical behavior similar to that of fluids has earned pentamode metamaterials the name of metafluids.

Among different types of mechanical metamaterials, pentamode metamaterials are principally important as any thermodynamically admissible elasticity tensor could be achieved through the consolidation of multiple pentamode topologies into one single lattice based topology. The pentamode metamaterials can be utilized as a general platform for rational design of metamaterials with any desired elasticity tensor. Besides, the bulk modulus of pentamode metamaterials can be decoupled from their mass density. The decoupling of mass density and elastic property further offers design flexibility of mechanical metamaterials. Hence, a pentamode structural platform is practically important to rationally design metamaterials.

Three-dimensional pentamode metamaterials in mechanics may be deemed as a counterpart of 3D magneto-dielectric metamaterials in optics. In 3D transformation optics, magneto-dielectrics enable anisotropies without birefringence and hence an optical wave impinging onto magneto-dielectric metamaterials with a certain polarization also emerges with that polarized direction and does not generate waves with other polarizations. While in pentamode metamaterials, there are only compressive waves but no shear wave transmission since shear waves are decoupled from the compressive waves and filtered or cloaked due to ignorable shear modulus.

A material with a very small shear modulus can flow away under shear stress in a way similar to a fluid [37,190]. For mechanical cloaking, macroscale pentamode lattices with different modulus ratios of  $(K/G)$  can be combined to render a physical object unfeelable [58]. Fig. 14 illustrates the structural features of pentamode metamaterials and their cloaking functions [58,107]. Fig. 14(a) shows the structural model approximate to the ideal pentamode material proposed by Milton and Cherkaev [107]. Cones touch each other at their thin ends with diameter  $d$  and connection points form a diamond lattice. Pairs of cones are connected at their thick ends with diameter  $D$ . The stable four-leg structure is a basic unit cell of the pentamode metamaterial. Owing to stress concentration near the cones, mechanical strength of the pentamode metamaterial mainly depends on the tip diameter  $d$ . The local bulk modulus  $K$  can be tuned via diameter  $d$  of the double-cone connections with respect to the fixed lattice constant  $a$ . Fig. 14(b) illustrates the corresponding body-centered cubic Brillouin zone where the characteristic points are indicated for interpretation of the corresponding band gap structures [56]. Fig. 14(c) depicts a rigid hollow cylinder embedded in a homogeneous 3D pentamode metamaterial environment (white) which is covered by a compliant pentamode metamaterial shell (red). An object placed inside of the hollow interior becomes unfeelable. In Fig. 14(c), an enlarged view is presented to clearly demonstrate the cloaking details of the pentamode metamaterial.

### 2.5.3. Fabrication and application to vibration and sound control

In theory, all conceivable 3D mechanical materials can be conceptually built from pentamode materials. However, pentamode materials had not been realized experimentally until 2012. Kadic et al. [190] discussed approximate fabrication of 3D pentamode microstructures using lithography and showed that a ratio of pentamode's bulk modulus to the shear one can be practically made as large as about 1000. They indicated that the theoretical ideal of pentamode materials suggested by Milton and Cherkaev [107] could be approximately fabricated using the advanced lithography.

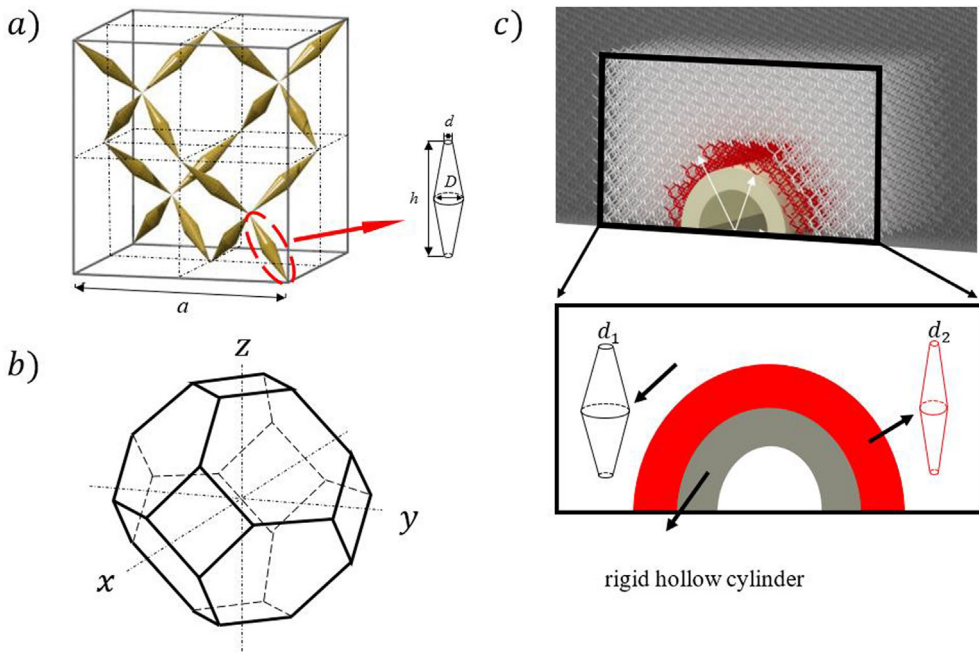


**Fig. 14.** Structural features of pentamode metamaterials and cloaking functions: (a) pentamode metamaterial unit cell, (b) a body-centered cubic Brillouin zone, and (c) a rigid hollow cylinder embedded in a homogeneous three-dimensional pentamode metamaterial and an enlargement view of the cloaking details of the pentamode metamaterial.

Martin et al. [56] studied the phononic band structures of three-dimensional pentamode metamaterials and found that compressive and shear waves could exhibit different phase velocities with more than one order of magnitude and the frequency intervals would be more than two octaves bandwidth. Kadic et al. [57] studied several theoretical possibilities to introduce intentional anisotropy into 3D pentamode metamaterials. In the dynamic case, uniaxial pentamode metamaterials could deliver anisotropic longitudinal wave phase velocities which were different by nearly one order of magnitude for realistically accessible microstructure parameters. Inspired by invisible core-shell nanoparticles in optics, Bückmann et al. [58] designed an approximate elasto-mechanical core-shell unfeelable cloak by using pentamode concepts. The 3D polymer microstructures were fabricated by rapid dip-in direct laser writing optical lithography and the measured displacement fields showed very good cloaking performance.

Kadic et al. [191] proposed a class of linear laminated metamaterials whose effective bulk modulus and mass density can be adjusted independently over a large range. Tian et al. [192] presented a broadband and highly transparent acoustic metasurface based on a frequency-independent generalized acoustic pentamode metamaterial to redirect refracted waves, in which the pentamode metamaterial was used to improve impedance matching between the metasurface and the background medium. Amendola et al. [193] studied the mechanical response under large elastic strains of pentamode layers confined between stiffening plates, and explored their potential applications as seismic and vibration isolation systems as well as impact protection devices.

Mechanical metamaterials exhibiting peculiar mechanical properties are originated from their topological design. Pentamode metamaterials are of paramount importance because they could be used as a design platform to possess any thermodynamically admissible elasticity tensor. Fraternali and Amendola [194] examined mechanical behaviors of metamaterials alternating pentamode lattices and stiffening plates, and showed that pentamode lattices could be employed as seismic isolation devices by suitably designing the lattice geometry and the joint stiffness. Hedayati et al. [195] fabricated the metallic pentamode metamaterials from a biocompatible and mechanically strong titanium alloy where the elastic modulus and yield stress were decoupled from their relative density.

As discussed above, pentamode materials can behave approximately as tailor-made artificial liquid. Recently, microscopic scale materials of this intricate structure were fabricated, and the static mechanical tests revealed that a very large ratio of material's bulk modulus to the shear one could be obtained so that the material properties could be approximated to those of liquid. Zhao et al. [196] designed and tested water-like 2D pentamode metamaterials. A water-like 2D pentamode material sample was fabricated based on a single metallic material and the centimeter scale sample was a hollow metallic foam-like structure. It was shown that this pentamode metamaterial could mimic water in acoustic properties over a wide frequency range, which may be used for designing metamaterial lenses and vibration isolation.

Cai et al. [197] numerically simulated the phononic band structures of Bragg scattering and locally resonant pentamode metamaterials containing the symmetric double-cone elements using finite element analysis. Goldsberry and Haberman [118] numerically analyzed a honeycomb structure composed of a doubly periodic array of curved beams using finite ele-

ment analysis. They indicated that the honeycombs with nonlinear stiffness elements could be used as tuneable elastic metamaterials. The nonlinear static elastic response that resulted from large deformations of the honeycomb unit cell could lead to a large variation in elastic wave dispersion associated with infinitesimal motions.

Guo et al. [198] studied topological guiding of elastic waves in phononic metamaterials on the basis of the 2D pentamode structures. They built phononic structures in silicon with protected propagation of elastic waves that resisted to the back scattering. Zhang et al. [199] numerically and experimentally investigated the mechanical properties of honeycomb pentamode materials fabricated by laser additive manufacturing and proposed the optimization strategy to rationally design pentamode metamaterials. Cai et al. [200] presented an approach for tuning the first phononic band gaps of locally resonant pentamode metamaterials based on the equivalent relationship between the locally resonant mode at the lower edge of the first phononic band gaps and the spring-mass system. Li and Vipperman [201] proposed a kind of pentamode material composed of three-dimensional hexagonal unit cells built with double-cone structures to create pentamode metamaterials with spherical geometries. This type of pentamode metamaterial with band gaps for shear waves might be used for acoustic cloaking applications. Although pentamode materials have been extensively studied and shown their potential applications since 1995, their fabrication and applications to vibration control need to be further investigated.

### 3. Origami-based structures

Following the brief introduction given in Section 1.3, more details on origami patterns, kinematic relationships, and their applications to vibration isolation will be discussed in this section. Origami, the ancient paper folding art of Japan, has inspired to design origami-based structures and devices for various engineering applications for several decades [76,77,202,203]. By adopting the new origami-based design techniques, various origami-based structures with multi-stable states have been developed [60,61,203]. The properties of origami structures highly depend on the folding patterns (base structures) which can be different according to their geometrical features and kinematic relationships.

#### 3.1. Common crease patterns and folding parameters

Mechanical properties of origami structures strongly rely on the geometric characteristics of the crease patterns, which will be discussed in this subsection. There are many crease design patterns that can be applied to practical engineering, including generic degree-4 vertex pattern, Miura-ori pattern, the stacked Miura-ori (SMO) pattern, the Tachi-Miura polyhedron (TMP) pattern, and waterbomb base pattern, cylindrical pattern and the other patterns. The origami architectures, generated from these patterns, will be referred to here as origami base structures. It should be mentioned that there are other phrases widely used in the literature, such as origami base, base element, and unit cell, in particular, unit cell is generally used in origami-based metamaterials. Sometimes, unit cells are alternatively referred to as base structures. Fig. 15 shows the examples of the typical origami base structures which are simply formed by common crease patterns.

##### 3.1.1. Generic degree-4 vertex pattern

The base structure of the generic degree-4 vertex pattern is a structural element made of one central vertex and four parallel quadrilateral facets. It can possess one continuous degree of freedom for rigid folding [204]. Specifically, the well-known Miura-ori pattern, which possesses both flat-foldability and collinear folds, is also a member of the degree-4 vertex family. Fang et al. [205] studied the deformation mechanisms of the four types of generic degree-4 vertex base structures. They indicated that the proposed generic degree-4 vertex cell could achieve more deformation features than the conventional Miura-ori pattern, as it could provide the additional self-locking ability, tri-directional negative Poisson's ratios and shearing stiffness.

##### 3.1.2. Miura-ori pattern

The Miura-ori pattern is an auxetic structure, whose Poisson's ratio can be negative. It possesses both flat-foldability and single-collinearity [206]. Poisson's ratios of the standard Miura-ori patterned metamaterial structures are equal but opposite for in-plane and out-of-plane deformations of the structure [75]. There are other types of folding patterns that have been developed on the basis of the Miura-ori pattern such as the zigzag pattern [207,208]. In a typical Miura-ori base structure, outer dimensions including four folding parameters can be described by its smallest facet size and the dihedral fold angle  $\theta$ . The facet is normally a parallelogram with side lengths of  $a \times b$  and an acute angle of  $\gamma$ . By referring to Fig. 15(a), the folded pattern parameters can be determined by [75]:

$$\begin{cases} H = a \sin \theta \sin \gamma \\ S = b \frac{\cos \theta \tan \gamma}{\sqrt{1+\cos^2 \theta \tan^2 \gamma}} \\ L = a \sqrt{1 - \sin^2 \theta \sin^2 \gamma} \\ V = b \frac{1}{\sqrt{1+\cos^2 \theta \tan^2 \gamma}} \end{cases} \quad (25)$$

where geometric parameters  $H$ ,  $S$ ,  $L$  and  $V$  are shown in Fig. 15(a). Parameters  $\xi$ ,  $\psi$  and  $\varphi$  represent the angles between the facets and the reference planes. Their relationships are given by:

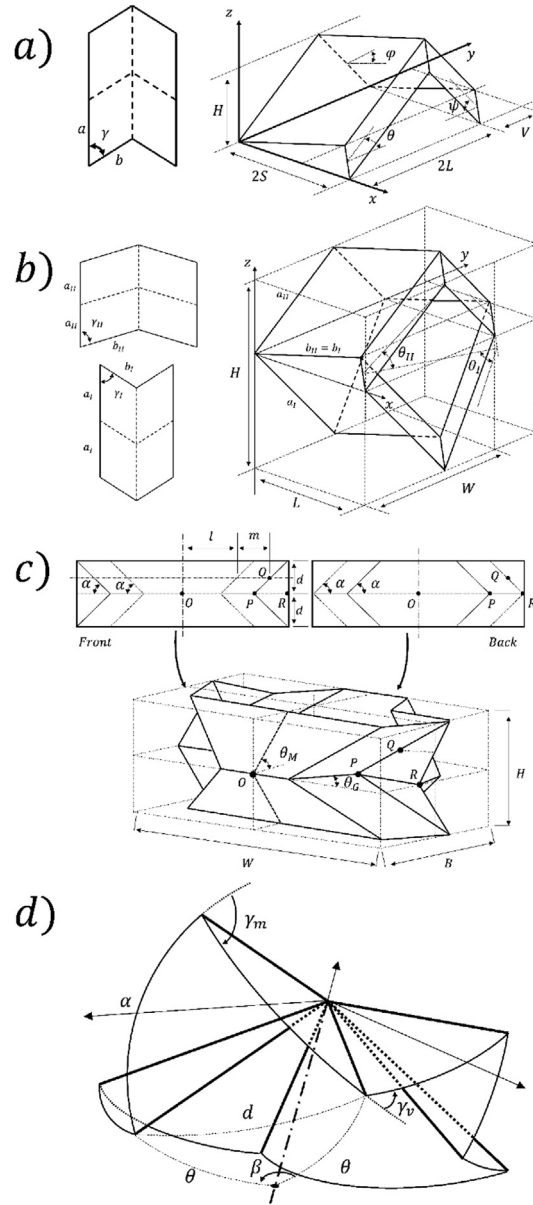


**Fig. 15.** Examples of typical origami base structures and their geometrical representations corresponding to different crease patterns: (a) generic degree-4 vertex pattern (Miura-ori pattern), (b) stacked Miura-ori (SMO) pattern, (c) Tachi-Miura polyhedron (TMP) pattern, and (d) waterbomb base.

$$\begin{cases} \tan \xi = \cos \theta \tan \gamma \\ \sin \psi = \sin \theta \sin \gamma \\ \cos \gamma = \cos \xi \cos \psi \\ \sin \varphi = \sin \xi / \sin \gamma \end{cases} \quad (26)$$

The negative in-plane Poisson's ratio ( $\nu_{in-plane}$ ) of the Miura-ori pattern can be characterized by measuring strains of the base structure during the folding motion. The out-of-plane Poisson's ratio ( $\nu_{out-of-plane}$ ) can be equal but opposite to that of the in-plane deformation. Constraints are normally required for the Miura-ori pattern without facet bending. The twisting or saddle-shaped deformation can be generated when the bending stiffness of the facets is not larger enough than the crease bending stiffness [75]. The Possion's ratios can be calculated as:

$$\begin{cases} \nu_{in-plane} = -\tan^2 \xi \\ \nu_{out-of-plane} = -\nu_{in-plane} \end{cases} \quad (27)$$

There are other folded shell structures with opposite behaviours on the in-plane and out-of-plane Poisson's ratios. For example, an egg box base structure has the positive in-plane Poisson's ratio and the negative out-of-plane Poisson's ratio. In general, such egg box base structures are not flat.

### 3.1.3. Stacked Miura-ori pattern

The stacked Miura-ori (SMO) pattern is formed by stacking different Miura-ori base structures (cells) to perform a foldable structure with intrinsic bi-stability [75,209]. Different origami patterns with the successive layout could exploit the fruitful geometry of the unit cell. The self-locking function could be enabled through specific configurations [210], which could provide effective mitigation under impact by the self-assembly technique. Fang et al. [204] investigated the dual-component design of the SMO structure based on the generic degree-4 vertex pattern to achieve a programmable self-locking feature and special stiffness property. For the SMO-based structure combined by at least two layers of different Miura-ori bases (unit cells) shown in Fig. 15(b), two different unit cells share the same designing parameters at the connecting planes and include at least one independent parameter. The expansion coefficients are then different from those of the standard Miura-ori pattern and can be re-written as [211]:

$$\begin{cases} L = \frac{2b_I \cos \theta_I \tan \gamma_I}{1 + \cos^2 \theta_I \tan^2 \gamma_I} \\ W = 2a_I \sqrt{1 - \sin^2 \theta_I \sin^2 \gamma_I} \\ H = a_I \sin \gamma_I \left( \sqrt{\frac{\tan^2 \gamma_{II}}{\tan^2 \gamma_I}} - \cos^2 \theta_I - \sin \theta_I \right) \end{cases} \quad (28)$$

where parameters  $L$ ,  $W$  and  $H$  are indicated in Fig. 15(b).

The joint edges of the top sheet (sheet II) and bottom sheet (sheet I) share the same facet side ( $b_I = b_{II}$ ), and the other edges of each sheet are independent ( $a_I, a_{II}$ ). The enclosed internal volume within a SMO base structure (unit cell) can be calculated according to its folding conditions as [212]:

$$V = 2a_I^2 b_I \sin^2 \gamma_I \cos \theta_I \left( \sqrt{\frac{\tan^2 \gamma_{II}}{\tan^2 \gamma_I}} - \cos^2 \theta_I - \sin \theta_I \right) \quad (29)$$

### 3.1.4. Tachi-Miura polyhedron pattern

Tachi-Miura polyhedron (TMP) pattern is a rigid folding origami base structure with the nonlinear stiffness developed on the basis of Miura-ori pattern [213]. With lateral assembly of small Miura-ori base structures into one single integrated unit, a certain volume can be held within the TMP base structure. Since the structure only deforms along the crease lines and does not rely on the material elasticity of its facets, the facets are completely rigid during the folding process. Yasuha and Yang [213] analytically and experimentally studied the Poisson's ratio and bi-stability of the TMP-based structure. Nonlinear stiffness and dynamic response of the TMP structure were discussed in [214]. As illustrated in Fig. 15(c), a certain volume in the unit could be changed within a full folding motion cycle. The minimum volume can be zero. The outer dimensions of the TMP pattern are obtained from its flattened sheet parameters and folding angles as [213]:

$$\begin{cases} B = 2m \sin \theta_G + d \cos \theta_M \\ W = 2l + \frac{d}{\tan \alpha} + 2m \cos \theta_G \\ H = 2d \sin \theta_M \end{cases} \quad (30)$$

where the geometric parameters  $B$ ,  $W$ ,  $H$ ,  $l$  and  $m$  are given in Fig. 15(c).

It is interesting to note that in-plane Poisson's ratios of the TMP base structure with respect to either width  $B$  or  $H$  are different [213]:

$$\begin{cases} v_{HW} = -\frac{dW/W}{dH/H} = -\frac{4m \tan \alpha \sin \theta_G \cos^2 \frac{\theta_G}{2}}{2l + \frac{d}{\tan \alpha} + 2m \cos \theta_G} \sin \theta_M \tan \theta_M \\ v_{HB} = -\frac{dB/B}{dH/H} = \frac{4m \tan \alpha \cos \theta_G \cos^2 \frac{\theta_G}{2} + d}{2M \sin \theta_G + d \cos \theta_M} \sin \theta_M \tan \theta_M \end{cases} \quad (31)$$

From the above equations, it can be calculated that Poisson's ratio in the HW plane (the front plane as shown in Fig. 15(c)) would always be less than zero. Meanwhile in the HB plane (the side plane), Poisson's ratio could drop to zero and remains at the low level when the folding ratio increases.

### 3.1.5. Waterbomb base

A waterbomb base is a single-vertex origami structure, which is normally folded from a square or circular sheet, as illustrated in Fig. 15(d). At least three groups of creases should be involved and each group includes one mountain and one valley. Characteristics of the waterbomb base include developable vertices, completely rigid facet, and rotationally symmetric geometry [215]. For a traditional  $n$  degree waterbomb base containing  $n$  pairs of mountain and valley folds, the geometric relationships for angles are given by:

$$\begin{cases} \alpha = 180^\circ/n \\ \beta = 360^\circ/n \\ 0 \leq \theta \leq 180^\circ - \alpha \end{cases} \quad (32)$$

where  $\alpha$  is the facet sector angle,  $\beta$  denotes the angle between any two folds that are the same type, and  $\theta$  is the angle between the valley fold and the reference central axis.

The dihedral angles at the creases can be found according to the folding types of mountains or valleys as [216]:

$$\begin{cases} \gamma_m = -180^\circ + \cos^{-1}\left(1 + \frac{\cos d - 1}{\sin^2 \alpha}\right) \\ \gamma_v = -180^\circ + 2\cos^{-1}(\cot \alpha \tan \frac{d}{2}) + 2\cos^{-1}(\cot \theta \tan \frac{d}{2}), \text{ if } \theta \leq 90^\circ \\ \gamma_v = 180^\circ - 2\cos^{-1}\left[(\cos d - 1) \frac{\cot \theta}{\sin d}\right] + 2\cos^{-1}(\cot \alpha \tan \frac{d}{2}), \text{ if } \theta > 90^\circ \end{cases} \quad (33)$$

where  $d$ ,  $\theta$  and  $\alpha$  represent the sector angles.

### 3.1.6. Cylindrical pattern and the other patterns

Cylinder-shaped origami structures normally have thin shells and can be buckled in twisting under torsional loadings. The cylindrical pattern can employ different base structures, including Kresling pattern [217], cylindrical Miura-ori base structure [218], and polygonal tubes [92,93,219]. Some other patterns have been developed according to different applications. Examples of the other patterns with compliant mechanisms and unique kinematics responses include diamond-cell [93,220], kite-shape [221], crash box cell [92,222], Kaleidocycle-inspired pattern [223], Yoshimura pattern [224], and bio-inspired morphing structures [49,225–227].

## 3.2. Design of origami structures

In designing an origami-based structure to satisfy requirements of practical applications, possible features of the origami base structures and suitable stability techniques should be considered. Magleby et al. [228] proposed a stability integration method to distinguish the origami structures, in which four groups of existing stability techniques were categorised based on the origami bistable conditions and the energy storage behaviours. In general, the design of origami structures includes pattern design, crease design, facet design, and kinematics modelling. Common origami patterns were given in Section 3.1, and the other design aspects of origami structures will be discussed in the following subsections.

### 3.2.1. Crease design

There are two basic components in the classic origami base structure, namely, creases and facets. Facets are joined by creases to form a unit cell (element). The crease design determines how the facets would be folded and deployed. A crease made of elastic materials provides torsional actuation for the facets to rotate about the crease during folding and deploying processes. Normally the crease is straight for a rigid origami pattern and thus the facets can be folded and deployed without deformation. There are two common crease models used in designing origami structures, namely, the hinge model and the bending model [76], as illustrated in Fig. 16. The mechanism of the hinge model is the use of active materials as the torsional and bending stiffness at the crease to drive the connected facets. In this model, the crease is a straight line with zeroth-order geometric continuity, which has been employed in the majority of the current rigid origami structures [229,230]. However, the bending stiffness at the crease of the hinge model would require revaluation if the crease range or material is changed. An evaluation on mechanical response of the different active crease materials has been conducted by using more compliant models in addition to the single torsional spring in [215,231–234]. In contrast to a traditional hinge model, a compliant joint could be more appropriate to approximate the fold of origami mechanisms [235,236]. An improved three-spring compliant crease model can be used to capture the torsional deformations of the creases and the extensional stretching energy of the origami structures [237]. The other modelling method, the bending model, is based on the bending deformation of the materials within the crease range. The advantage of the hinge model type is the massive foldability. However, the driving field for folding can be difficult to be defined, unless it is mechanically constrained. Fig. 16(b) illustrates a pseudo-rigid-body model to design origami structures. The rotational stiffness  $k_{crease}$  of the single compliant crease can be expressed as:

$$k_{crease} = \frac{E_{crease} L t^3}{12 W} \quad (34)$$

where parameters  $L$ ,  $W$  and  $t$  represent the length, width and thickness of the crease model, and  $E_{crease}$  is Young's modulus of the crease material.

Fig. 17 shows the geometric continuity and non-zero thickness solution for the origami structure with non-negligible fold thickness. Modelling of an origami structure is usually conducted by neglecting facet thickness as shown in Fig. 17(a). For the origami structures with non-negligible fold thickness, this simplification is inappropriate due to the possible physical conflicts of the materials. In this case, a higher-order geometric continuity model or the smooth fold model can be used as shown in Fig. 17(b). Peraza Hernandez et al. [238,239] presented a model exhibiting the higher-order geometric continuity, also known as smooth folds, for rigid origami structures with nonzero thickness folds. Geometric methods, such as membrane

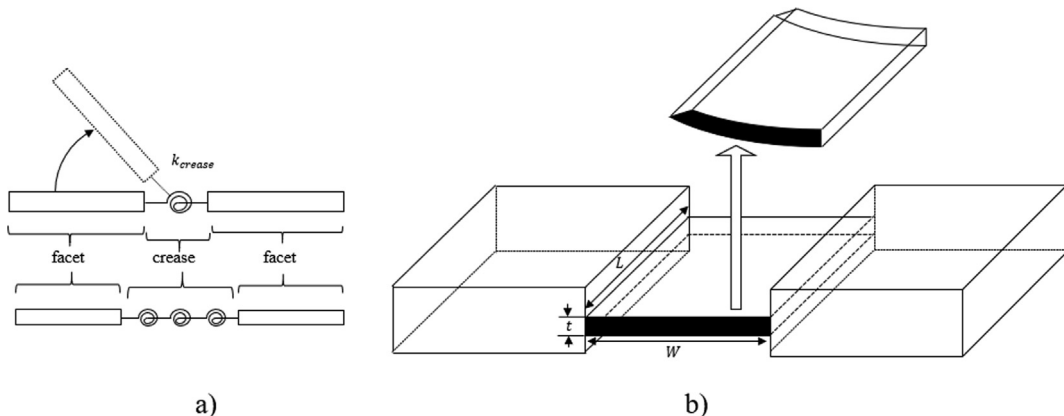


**Fig. 16.** Hinge and bending models of creases in an origami base structure: (a) torsional spring (top) and improved three-spring compliant crease model (bottom), and (b) the pseudo-rigid-body bending model.

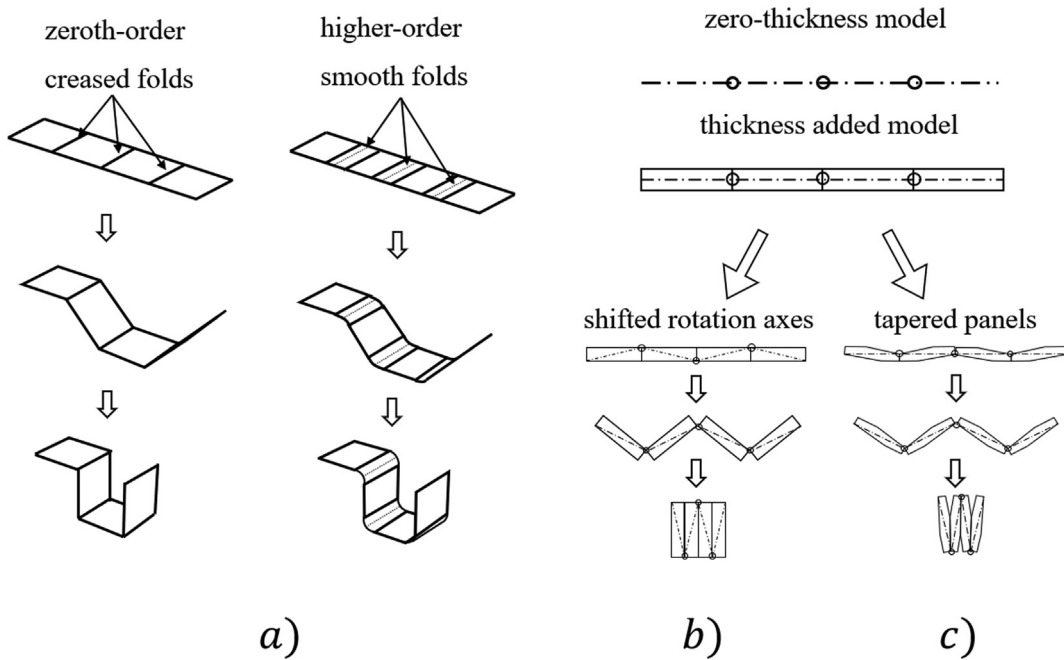


**Fig. 17.** Geometric continuity and non-zero thickness folds: (a) the zeroth-order geometric continuity and the higher-order geometric continuity, (b) the shifted rotation axes, and (c) the tapered panels method.

gaps [240], tapered panels [241], offset panels [242], and offset creases [243,244] have been developed to reduce the thickness effect on the hinge model in engineering applications.

There are other crease types that can be used to design origami structures. Hanna et al. [216] used the split-fold crease to design a waterbomb base with bistable states and showed that the split-fold waterbomb base structure has lower force response and potential energy as compared to the traditional waterbomb base in the bi-stable state transition.

### 3.2.2. Facet design

In the design of rigid origami pattern, mobility of the crease and the rigid foldability should be examined to confirm with the rigid origami requirement [245] no matter whether the facets of the origami pattern are bent or not during the deployment. Silverberg et al. [246] reported the hidden degree of freedom (DOF) of the facet finite bending during the deployment. Different methods can be used to check the hidden DOF for different geometrical characteristics of the origami pattern. Wu and You [247] constructed a rotating vector model for a general origami element using the quaternion theory on the spatial fixed-point rotations, referring to as the quaternion rotation sequence method. As this method may not be suitable for the

cylindrical patterned structure, Cai et al. [248] combined the quaternion rotation sequence and dual quaternion method to examine the rigid foldability of the foldable structure. Cai et al. [249] found that although the folding angles of the Kresling-pattern could meet with the requirement of the rigid foldability, its coordinate relationship would not meet with the requirement, meaning that the Kresling-pattern is not rigidly foldable.

In order to study the compliance of the facets in the rigid origami structures, Rommers et al. [250] used the pseudo-rigid-body model, as shown in Fig. 16(a), to incorporate stiffness performance of a single vertex compliant facet origami mechanism, where the compliant facets were divided into two rigid facets using virtual hinge connections with torsional stiffness. Different joint methods were tested to manipulate the moment curve of the single vertex compliant facet mechanism for the origami design in [251]. Yu et al. [252] used the thin plate bending theory to study the deflections of the facets in the Miura-ori base structure and obtained the deflection curves of the facets under different stress conditions. Zimmermann et al. [253,254] discussed the rigid and flat foldability of  $n$  vertices through the kinematic model.

### 3.2.3. Kinematic modelling

In order to study origami kinematics, spherical mechanism [255], especially the spherical lamina emergent mechanism [256] or known as a spherical 4R linkage model, is usually used. In this model, each vertex in the origami pattern is equivalent to a centre of the spherical model and the creases are represented by lines. Bowen et al. [257] proposed a classification scheme for the origami structure based on the spherical mechanism. Liu et al. [258] proposed a four-crease single-vertex unit pattern to derive the prismatic origami structures where the spherical 4R linkage model was used to represent the pattern system. As illustrated in Fig. 18, the crease fold lines can be shared between two spherical mechanisms. Multilayer of a closed loop of the unit pattern can form a  $2n$  sided prismatic origami structure with both straight and curve variations in one DOF. Truss model can also be used to describe the origami kinematics, particularly for the Kresling pattern [217,259–262]. Cai et al. [261] considered the creases as bar elements and studied the elastic strain energy during the folding and deploying processes.

For all types of origami base structures, the folding angles at the creases and the geometric parameters can be used to calculate the potential and kinematic energies of the structure. The total elastic energy is induced by bending deformations of both creases and facets [246]:

$$U_{\text{total}} = U_{\text{crease}} + U_{\text{facet}} \quad (35)$$

For the rigid-origami structure, only the potential energy of the creases is important. The elastic potential energy of an origami base structure is a summation of each individual crease's energy, which can be calculated by its dihedral angles  $\gamma_{\text{crease}}$  of the creases and its corresponding torsional stiffness  $K_i$  as [263]:

$$U_{\text{crease}} = \frac{1}{2} \sum_{i=1}^n K_i (\gamma_i - \gamma_i^0)^2 \quad (36)$$

where  $\gamma_i^0$  represents the initial dihedral angles of the creases, which is assumed to be in stress-free states.

Meanwhile, there exists total kinetic energy  $T_{\text{facet}}$  within the base structure due to the facet's absolute motion during the folding process:

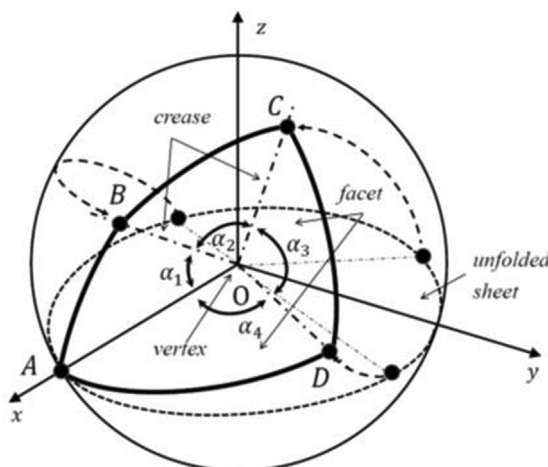


**Fig. 18.** The spherical mechanism with single vertex origami structure.

$$T_{facet} = \frac{1}{2} \sum_{i=1}^n m_i V_{cm}^2 \quad (37)$$

where  $m_i$  denotes the mass of each facet, and  $V_{cm}$  represents the absolute velocity of the facet at its mass centre.

The calculation of both potential and kinematic energies of the origami structures is generally used to analyse the energy distribution of the structure, which provides useful information for applying the origami structure to vibration control.

### 3.3. Dynamic modelling and vibration control

As discussed in [Sections 3.1 and 3.2](#), important characteristics of origami structures include auxetics, bi- and multi-stability, which are useful to absorb and dissipate dynamic energy in vibration attenuation. This section discusses dynamic modelling and vibration isolation by using origami-based structures.

#### 3.3.1. Dynamic behaviour

The resonant frequencies of origami structures are closely related to their stable states and the dynamic response of origami structures depends on their patterns, deployed stable states, and direction of the external excitation. Hanna et al. [215] analysed the kinematic and potential energies of a symmetric waterbomb base, and studied the equilibrium states and the force-deflection response during the deploying motion. They indicated that the bi-stable states could be controlled by changing the stiffness of the creases. Sadeghi and Li [264] found that intra-well resonance frequencies of the waterbomb based origami structure were different at its two stable states, and derived the equations of motion and the time response under harmonic excitations. [Fig. 19](#) shows the dynamic response of the waterbomb based origami structure under intra-well oscillations [264].

Yasuda et al. [214,265] studied the dynamic behaviour of a lattice structure with the Tachi-Miura polyhedron (TMP) pattern under harmonic excitations. A simple multi-bar linkage model was used to simulate dynamic performance of the TMP unit structure and compared with the lumped mass model. The tuneable frequency band could be achieved by either changing parameters of the identical TMP base structure or combining different TMP base structures. This kind of origami-based metamaterial structures could be potentially used to control vibrations and impacts after modifying the designs to enhance the features for vibration isolation.

The structural nonlinearity of stacked Miura-ori (SMO) base structure is dominated by the quadratic and cubic components. Sengupta and Li [266] carried out a geometrically-parametric analysis for the SMO structure and indicated that the length ratio between crease lines and sector angle is one of the key designing parameters significantly affecting the system stiffness. Fang et al. [209] investigated the dynamic response of the bi-stable SMO structure under both the intra-well and inter-well harmonic excitations, and revealed that the nonlinearities of the SMO structures were dominated by quadratic and cubic terms in its equation of motion. Xia et al. [267] further analysed the dynamic response of the SMO structure under harmonic oscillations and compared with similar origami structure such as the stacked single-collinear origami structure. [Fig. 20](#) illustrates energy profiles of the SMO-based origami structure and the Helmholtz-Duffing oscillator [209]. Similarity of the energy profiles to the Helmholtz-Duffing oscillator could be helpful for further development of origami structures.

The unique kinematic feature of the SMO-based structure can lead to asymmetric behaviours when it is switched between different stable states. Fang et al. [263] proposed an asymmetric energy barrier based on SMO-based structures,

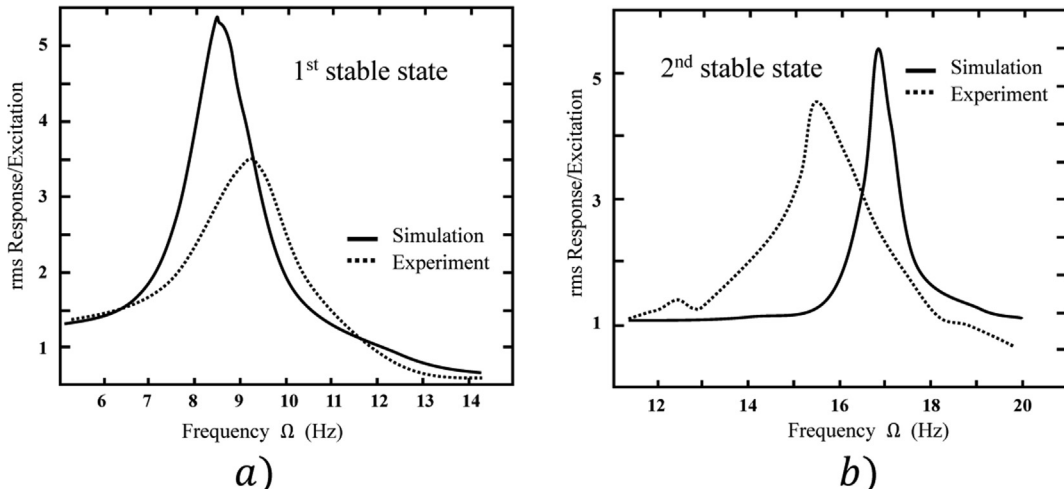


**Fig. 19.** Dynamic response of the waterbomb base unit under intra-well oscillations at: (a) the 1st stable state, and (b) the 2nd stable state.

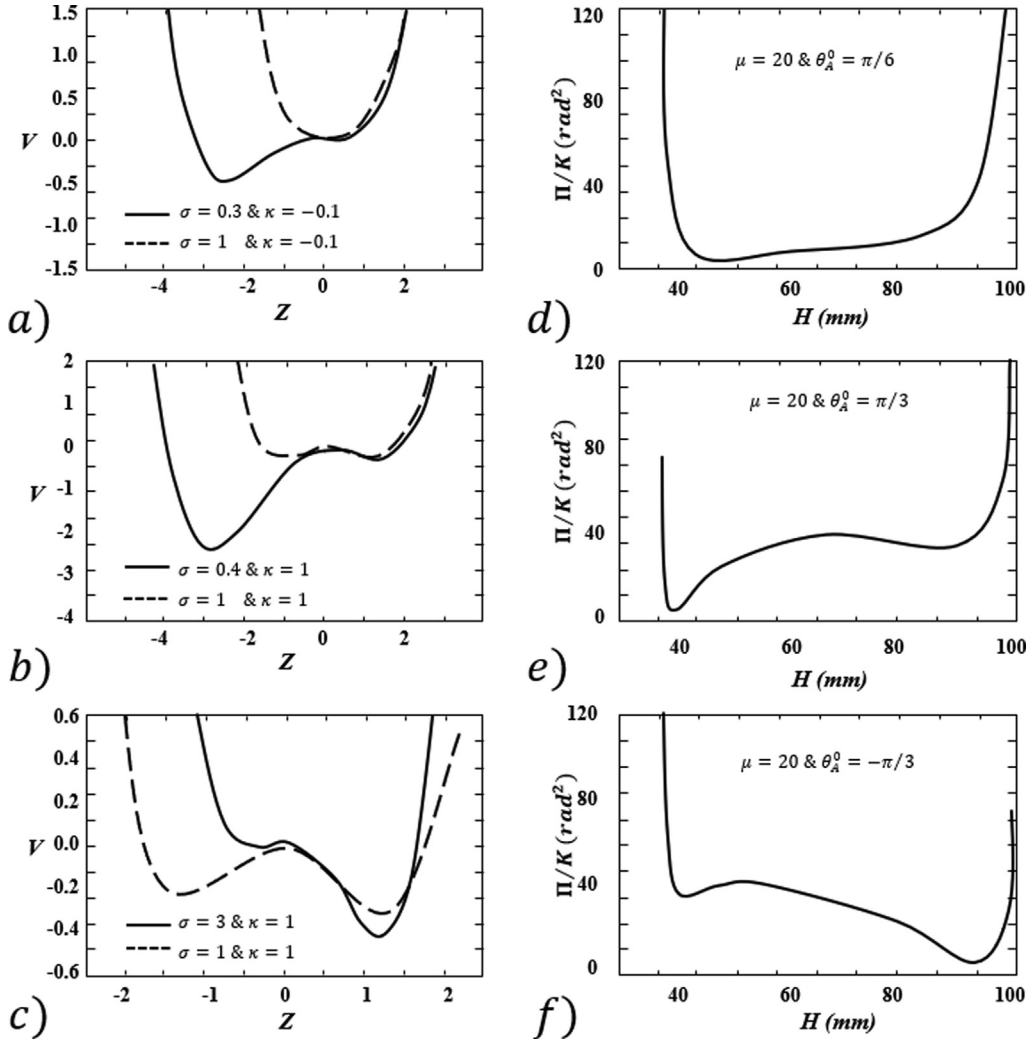


**Fig. 20.** Similarities of energy profiles between: (a-c) the SMO-based structure, and (d-f) the Helmholtz-Duffing oscillator.

in which two different bi-stable SMO cells were assembled into one unit cell to form a dual-cell chain with multi-stable states. Fig. 21 shows the energy landscape and the force-displacement relationship of the dual-cell chain SMO structure [263]. The energy landscape and the force-displacement relationship indicated that this dual-cell chain SMO structure required much larger extension force than the compression force to switch among the multi-stable states.

Most of the studies on dynamics of origami structures have focused on in-plane dynamic response, but the out-of-plane motion is also important in order to understand origami dynamics. Lv et al. [268] numerically investigated the response of the Miura-ori patterned sheets under the out-of-plane compressive excitations and studied the effects of the sheet thickness, side length, dihedral angles and sector angles on the dynamic response. A comparison between the response and the excitation would provide an evaluation on its vibration isolating performance.

Qiu et al. [269] studied the elastic behaviour of the creases to obtain the reaction force and investigated the force response of waterbomb based parallel origami structure under either translational-motion or rotational-motion. Sengupta and Li [211] exploited the anisotropy of a multi-cellular SMO structure to achieve an on-demand stiffness adaptation. The anisotropy of the SMO unit cell was arranged in terms of different stable and unstable states along each primary axis, as shown in Fig. 22 [211]. The energy landscapes (a-c) and force-displacement responses (d-f) along different directions show that the unstable equilibrium state demonstrates the largest deformation in both length and width directions. The standard SMO-based structure could be assigned to cellular level to dictate the effective modulus of the structure. For this proposed SMO-based origami structure, its elastic moduli depend on the number of unit cells as shown in Fig. 23 [211], in which the energy landscapes of both 2-cell chain and 3-cell chain are compared.

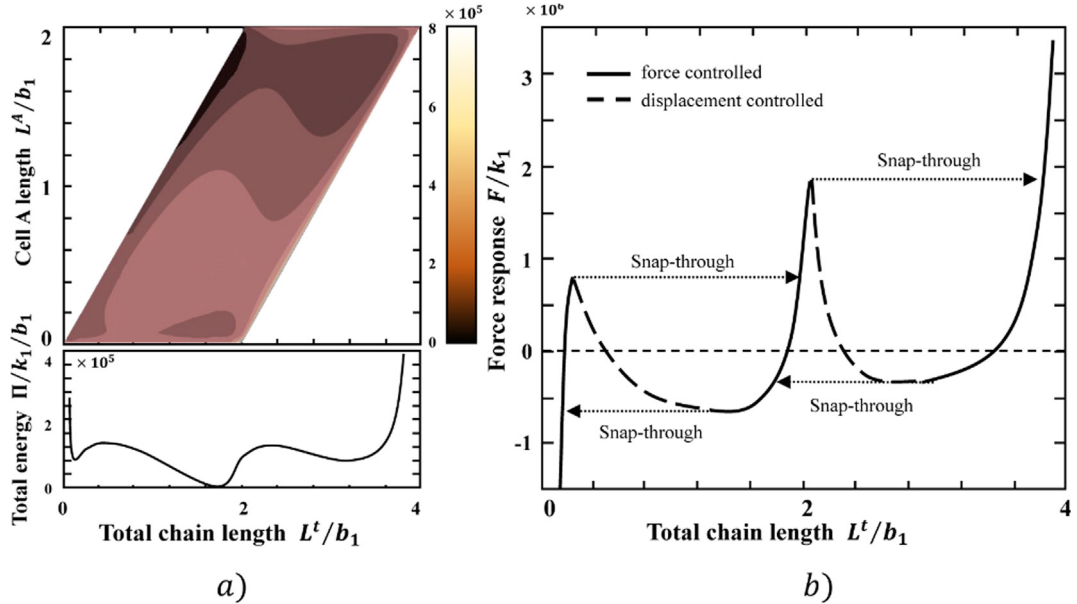


**Fig. 21.** Energy landscape and force–displacement curve of a dual-cell chain SMO-based structure: (a) Energy landscape, (b) Force-displacement curve.

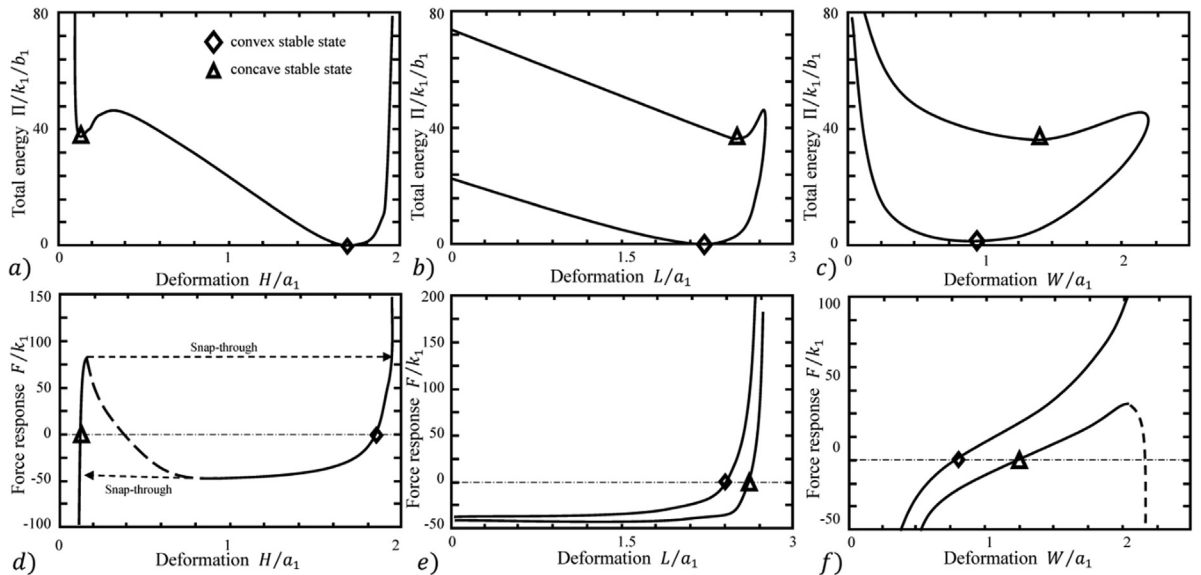


**Fig. 22.** The anisotropy of the SMO structure in the energy landscape (a-c), and the force response (d-f) with respect to the external deformations in height  $H$ , length  $L$ , and width  $W$  directions.

### 3.3.2. Origami-based QZS isolator

The nonlinearities of the force–displacement responses of the origami structures can also achieve the high-static-low-dynamic stiffness characteristic as a nonlinear QZS vibration isolation system. Fig. 24 presents two examples of the force–displacement curves from the fluidic origami structure [270] and the SMO-based origami structure [267].

When the tubular volume of the SMO origami structure is filled by fluid, mechanical performance of the origami structure can be controlled by fluid pressure. Li and Wang [212] proposed the fluidic origami structure by filling the tubular volume with high bulk modulus fluid, in which a truss frame was used to model the structure. Different from the typical SMO structure with the unconstrained tubular volume, the fluidic origami with the constrained internal fluid system can produce tunable stiffness characteristics, though an additional fluidic system is required to supply the fluid flowing within the origami structure. Sadeghi and Li [270] investigated the pressurized fluidic origami structure with the QZS feature, and experimentally verified vibration isolation by using the QZS characteristics. On the basis of the bi-stable property and the nonlinear

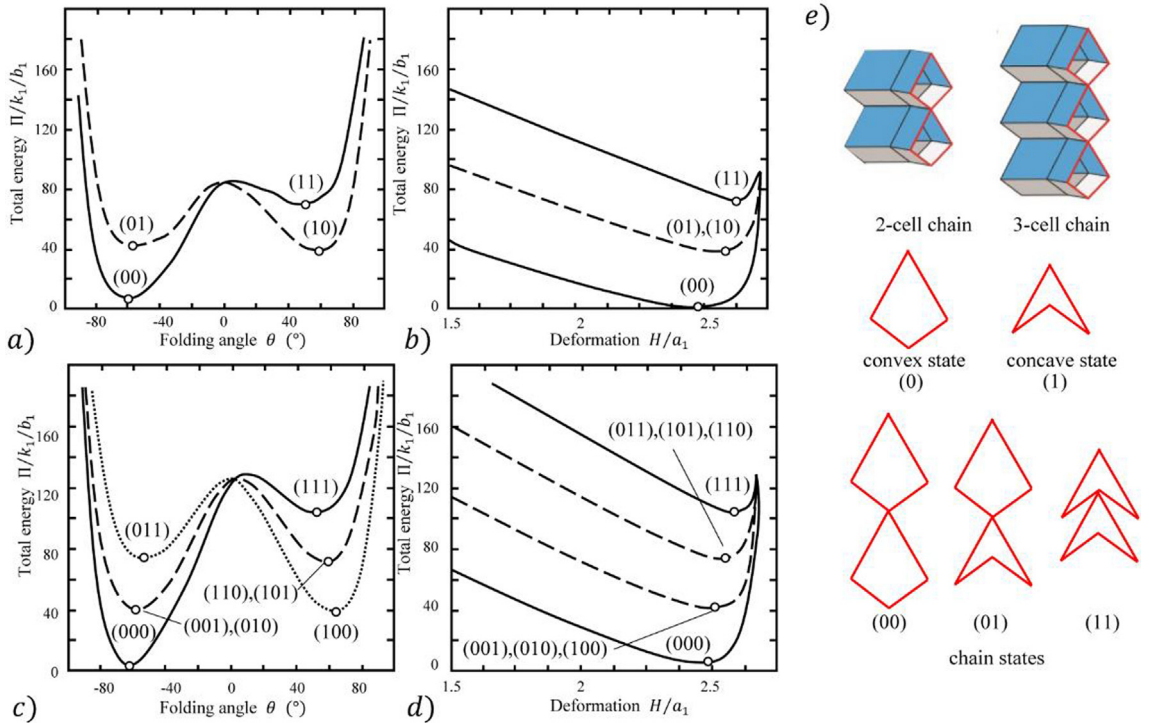


**Fig. 23.** Energy landscapes of (a-b) 2-cell SMO chain, (c-d) 3-cell SMO chain at different stable states, and (e) the chain states.

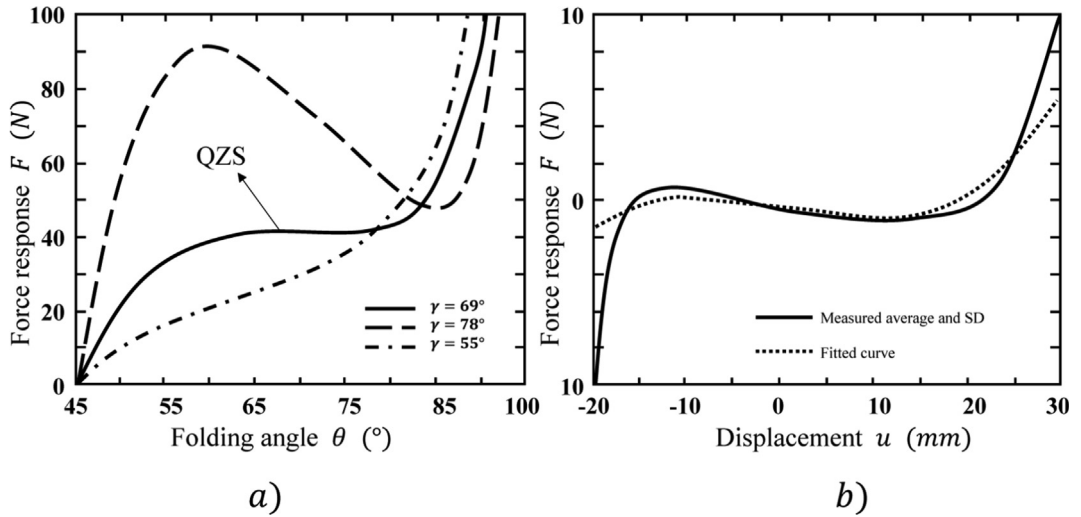


**Fig. 24.** Force-displacement response curves of origami structures: (a) fluidic origami structure, and (b) SMO-based structure.

stiffness characteristics of origami structures, Ishida et al. [259,260] developed a QZS vibration isolator using the Kresling-pattern foldable cylinder. The torsional buckling origami pattern was designed to act as the negative stiffness component in this QZS system. Rotational motions might be induced during the folding and deploying processes and thus the application of an external static load would be needed to avoid additional bending modes of the entire structure. Extension of the loading range of this origami-based QZS isolator for vibration isolation was achieved by adjusting the pre-compression of the main spring or changing the design variables of the origami base structure [271]. Meng et al. [272] proposed an origami-inspired multi-direction vibration isolator used in the momentum wheel assembly for satellites. In this isolator, Z-folded units were orthogonally arranged to provide lower stiffness in translation but high stiffness in rotation. Thus, the micro-vibration of the assembly in the translational direction could be isolated and the torque transmission could be retained.

Force-displacement curves in Figs. 22 and 24 show that origami structures can be tailored to design vibration isolation systems as different shapes of these curves can be achieved by properly designing origami patterns. Up to date, use of origami structures for vibration control and sound absorption is quite limited partially because of the challenges in design and fabrication of origami structures using conventional mechanical components available.

### 3.4. Fabrication of origami structures

It is noted that the traditional origami structure with folding and deploying states are generally difficult and expensive to be fabricated for engineering applications due to complexity. Different techniques have been developed for fabricating the origami structures. For instance, additive manufacturing by adding interior and boundary cuts could be used in 2D origami sheet to fabricate the desired non-flattenable 3D shape [273]. By pasting simple patterns using the Lego NXT (a robotic technique), the spherical 3D origami structure can be constructed directly [274]. The shape deposition manufacturing, the smart composite microstructure fabrication and a 3D printing technique were studied for manufacturing the origami wheel prototypes in [275]. The reversed torsion origami structure was developed to reduce the manufacture cost for the reversed spiral origami structure in [276]. However, a simple mechanical structure is still not yet designed to produce the tuneable stiffness feature of origami-based structures.

It should be mentioned that although the existing research has provided a solid foundation for implementing origami structures into engineering applications (potentially for vibration isolation), there are at least two challenges facing in real engineering applications: the material selection and the physical realisation of the structure. In many existing studies, the crease's deformation among its different states is normally large and can be flipped between "mountain" and "valley". This requires the materials to have the ductility and malleability necessary for the operating condition. The materials' fatigue life under high-stress working environment can also be a restriction to limit real applications. The other challenge is the physical realisation of the origami structure connecting to other components in real applications. It is noted that all facets and creases within the origami structure during its folding process are in movement, and the related spatial orientations are changed. This needs a proper design to connect the origami structure to the other non-origami components without any collision in the structures containing origami structure segments, during the folding and deploying process.

## 4. Concluding remarks

### 4.1. Summary

This paper has briefly reviewed the state-of-the-art research on mechanical metamaterials in terms of their peculiar mechanical properties and on origami-based structures with respect to their patterns, as well as on the applications of mechanical metamaterials and origami-base structures to vibration and sound control. It indicates that:

- 1) Cellular structures with negative stiffness components can be used to design and fabricate quasi-zero stiffness (QZS) isolators for vibration isolation;
- 2) Auxetic metamaterials have efficient dynamic energy absorption and dissipation capacities and thus are feasible for vibration and sound mitigation;
- 3) Band gap metamaterials are able to block stress waves with a certain range of frequencies or considerably attenuate wave propagation;
- 4) Pentomode metamaterials with near zero shear stiffness can stop or mitigate shear wave propagation; and
- 5) Origami-based structures with bi- and multi-stable states and nonlinear force–displacement relationships are of great potentials for formulating QZS isolators.

### 4.2. Challenges and further work

#### 4.2.1. Nonlinear analysis and negative properties

On the basis of the definition of Poisson's ratio, it is strictly restricted by linear elastic behaviour with small strain and the current study on negative Poisson's ratio focuses on the linear elastic range of the metamaterials. The linear range limitations are also assumed in the analysis of other metamaterials. Nevertheless, metamaterials used for vibration and sound mitigation may undergo large deformation or even work in a plastic region. In the QZS vibration isolators, negative stiffness components are essential and thus nonlinear analysis must be conducted to achieve the expected vibration isolation performance. There exist small-amplitude intrawell and large-amplitude interwell oscillations in the bi-stable structure to attenuate or amplify the vibrations in different frequency ranges. These vibration responses include single-periodic, sub-harmonic, and even chaotic components as the quadratic and cubic nonlinearities exist in the system. Therefore, nonlinear analysis is necessary and challenging to develop mechanical metamaterials and origami-based structures for vibration and sound control.

In addition to mechanical metamaterials with negative Poisson's ratio, the metamaterials with other negative properties have also been studied such as negative compressibility and thermal expansion. It is a challenge to combine various prop-

erties particularly negative material constants in a single mechanical metamaterial. Further study on mechanical metamaterials with negative properties and their physical essences are necessary for producing desired stiffness features and multi-stable states for vibration isolation.

#### 4.2.2. Fabrication, nano-scale and size effect, and test

Additive manufacturing technology has enabled the fabrication of metamaterials and origami-based structures with sophisticated features at multi-length scales that are impossible using conventional technologies. The recently developed advanced technologies of 3D printing, direct laser writing, self-propagating polymer waveguide and projection micro-stereo lithography have made it possible to synthesize metallic and ceramic micro- and nano-lattice metamaterials that have peculiar mechanical properties such as ultrahigh specific strength and stiffness, negative Poisson's ratio, pentamode and chirality. When the unit cell of the metamaterials is at a micro- and nano-scale, size effects on mechanical properties cannot be ignored, e.g., the size effect may induce a change in Poisson's ratio from positive to negative.

Advances in 3D printing techniques have made it possible to fabricate complicated material structures. Many of the designs of metamaterials discussed in this review can not only be carried out through theoretical and computational investigations, but can also be experimentally observed. Developing test and characterisation approaches using advanced techniques such as the DIC and 3D tomography coupled with in-situ mechanical testing platforms is essential to further understand the deformation mechanisms of metamaterials. Topology optimization is an effective tool to design metamaterials and origami structures with sophisticated geometrical configurations. One challenge is how to deal with the geometric complexity of 3D extremal mechanical metamaterials, such as 3D pentamode structures or plane pantographic metamaterials. The metamaterial and origami concepts combined with advanced 3D additive manufacturing technologies might further promote the generation of interesting mechanical metamaterials and origami-based structures in future studies, which may find applications in vibration isolation for nano-scale or small-sized devices and structures.

#### 4.2.3. Topology optimization and 3D metamaterials.

With an advance of 3D printing technology, topology optimization has been successfully used to optimally design metamaterials to achieve better mechanical behaviours. However, optimization objectives are mainly on compliance and compliant mechanism to design metamaterials with ultra-high stiffness or the specific property such as negative Poisson's ratio. Topology optimization to achieve optimal design of metamaterials for vibration and sound control is rare in the existing literature. Also, most of optimal designs of metamaterials in current studies are limited in 2D and linear analysis. The 3D optimal designs for nonlinear structures are necessary in order to find wide applications of mechanical metamaterials to vibration and sound control. Extending study on the mechanical behaviours of mechanical metamaterials to 3D and nonlinear analysis is expected to achieve fruitful scientific results in the future, which is expected to explore stiffness features in three-directions and thus offers promising structures for designing novel vibration isolators to prevent multi-directional vibrations transferred to the objects.

#### 4.2.4. Smart metamaterials and origami-based structures

Smart materials can play a significant role in the realization of self-folding and self-deploying origami-based structures. When the crease is fabricated by combining smart materials such as piezoelectric ceramics and shape memory alloy, folding and deploying states of the origami structures can be actively controlled by electric signals. There are many theories and software that could be used to design and analyze origami structures with zero thickness, but folding and deploying of origami structure with non-neglectable thickness is challenging and should be further studied for practical applications in which sheet thickness of origami pattern will not be several orders of magnitude less than sheet length scales. The bi-stable states and auxetic characteristics of origami structures have great potentials in various dynamic applications. Although a solid foundation for applying the origami structure in vibration control has been provided by understanding its kinematics, the force-displacement relationship and the energy profile of different patterns, the proof-of-concept prototypes of using the origami structures in engineering applications are rare to be found. Identifying the advantages of using origami-based structures over other structures for vibration and sound control could provide valuable insights for opening new avenues in real-world applications.

#### 4.2.5. Novel design and realization of origami-based structures

There is less available research on the use of origami-based structures to construct QZS vibration isolators. Though some existing studies have shown the origami-based structures could produce quasi-zero-stiffness and tuneable stiffness feature for vibration isolation, the proposed origami structures, such as pressurised fluidic origami cellular structure and Kresling pattern based cylindrical truss structures, may not be accepted for practical application because additional fluidic systems are required to incorporate into the origami mechanical structures, which makes the design more complicated and less attractive for engineering applications. Examples of using origami-based structures for vibration isolation is still lacking in real-world applications. A novel mechanical design is desirable to produce origami-based structures by using simple mechanical components such as beams, plates, bolts, springs. Bio-inspired design is also highly desirable to incorporate into the design of origami-based structures. The use of simple mechanical components to develop fully assembled origami-based structures for vibration isolation in practical engineering applications is crucial for the long term sustainability of the origami application in vibration control.

Although the peculiar mechanical properties of auxetic, band gap and pentamode metamaterials as well as origami-based structures are very promising in principle and many mechanical metamaterials and origami structures have been designed, fabricated and tested, very few of them have been applied to practical engineering, particularly in vibration and sound control. It is necessary to further explore applications of mechanical metamaterials and origami-based structures in this area. It is expected that novel vibration isolators will be designed by taking the advantages of the distinctive mechanical properties of both mechanical metamaterials and origami-based structures.

## Declaration of Competing Interest

The authors declare that they have no known competing financial interests or personal relationships that could have appeared to influence the work reported in this paper.

## Acknowledgments

This work is partially supported by the Australian Government through the Australian Research Council. The authors would like to thank the three anonymous reviewers for their helpful comments and suggestions.

## References

- [1] A. Carrella, M.J. Brennan, T.P. Waters, V. Lopes Jr, Force and displacement transmissibility of a nonlinear isolator with high-static-low-dynamic-stiffness, *Int. J. Mech. Sci.* 55 (2012) 22–29.
- [2] F. Zhao, J. Ji, K. Ye, Q. Luo, Increase of quasi-zero stiffness region using two pairs of oblique springs, *Mech. Syst. Sig. Process.* 144 (2020) 106975.
- [3] F. Zhao, J. Ji, K. Ye, Q. Luo, An innovative quasi-zero stiffness isolator with three pairs of oblique springs, *Int. J. Mech. Sci.* 192 (2021) 106093.
- [4] A. Carrella, M.J. Brennan, I. Kovacic, T.P. Waters, On the force transmissibility of a vibration isolator with quasi-zero-stiffness, *J. Sound Vib.* 322 (2009) 707–717.
- [5] R.A. Ibrahim, Recent advances in nonlinear passive vibration isolators, *J. Sound Vib.* 314 (2008) 371–452.
- [6] A. Carrella, M.J. Brennan, T.P. Waters, Static analysis of a passive vibration isolator with quasi-zero-stiffness characteristic, *J. Sound Vib.* 301 (2007) 678–689.
- [7] I. Kovacic, M.J. Brennan, T.P. Waters, A study of a nonlinear vibration isolator with a quasi-zero stiffness characteristic, *J. Sound Vib.* 315 (2008) 700–711.
- [8] X. Sun, X. Jing, Multi-direction vibration isolation with quasi-zero stiffness by employing geometrical nonlinearity, *Mech. Syst. Sig. Process.* 62 (2015) 149–163.
- [9] H. Ding, J. Ji, L.-Q. Chen, Nonlinear vibration isolation for fluid-conveying pipes using quasi-zero stiffness characteristics, *Mech. Syst. Sig. Process.* 121 (2019) 675–688.
- [10] C.C. Lan, S.A. Yang, Y.S. Wu, Design and experiment of a compact quasi-zero-stiffness isolator capable of a wide range of loads, *J. Sound Vib.* 333 (2014) 4843–4858.
- [11] Z. Hao, Q. Cao, The isolation characteristics of an archetypal dynamical model with stable-quasi-zero-stiffness, *J. Sound Vib.* 340 (2015) 61–79.
- [12] D. Xu, Y. Zhang, J. Zhou, J. Lou, On the analytical and experimental assessment of the performance of a quasi-zero-stiffness isolator, *J. Vib. Control* 20 (2014) 2314–2325.
- [13] X. Huang, X. Liu, J. Sun, Z. Zhang, H. Hua, Vibration isolation characteristics of a nonlinear isolator using Euler buckled beam as negative stiffness corrector: A theoretical and experimental study, *J. Sound Vib.* 333 (2014) 1132–1148.
- [14] N. Vo, T. Le, Adaptive pneumatic vibration isolation platform, *Mech. Syst. Sig. Process.* 133 (2019) 106258.
- [15] K. Ye, J. Ji, T. Brown, Design of a quasi-zero stiffness isolation system for supporting different loads, *J. Sound Vib.* 471 (2020) 115198.
- [16] C. Ren, D. Yang, H. Qin, Mechanical performance of multidirectional Buckling-based Negative Stiffness metamaterials: An analytical and numerical study, *Materials* 11 (2018) 1078.
- [17] J. Zhou, X. Wang, D. Xu, S. Bishop, Nonlinear dynamic characteristics of a quasi-zero stiffness vibration isolator with cam-roller-spring mechanisms, *J. Sound Vib.* 346 (2015) 53–69.
- [18] X. Tan, B. Wang, S. Chen, S. Zhu, Y. Sun, A novel cylindrical negative stiffness structure for shock isolation, *Compos. Struct.* 214 (2019) 397–405.
- [19] A. Guell Izard, R. Fabian Alfonso, G. McKnight, L. Valdevit, Optimal design of a cellular material encompassing negative stiffness elements for unique combinations of stiffness and elastic hysteresis, *Mater. Des.* 135 (2017) 37–50.
- [20] F. Zhang, S. Shao, Z. Tian, M. Xu, S. Xie, Active-passive hybrid vibration isolation with magnetic negative stiffness isolator based on Maxwell normal stress, *Mech. Syst. Sig. Process.* 123 (2019) 244–263.
- [21] B. Yan, H. Ma, L. Zhang, W. Zheng, K. Wang, C. Wu, A bistable vibration isolator with nonlinear electromagnetic shunt damping, *Mech. Syst. Sig. Process.* 136 (2020) 106504.
- [22] T. Zhu, B. Cazzolato, W.S.P. Robertson, A. Zander, Vibration isolation using six degree-of-freedom quasi-zero stiffness magnetic levitation, *J. Sound Vib.* 358 (2015) 48–73.
- [23] W.S. Robertson, M. Kidner, B.S. Cazzolato, A.C. Zander, Theoretical design parameters for a quasi-zero stiffness magnetic spring for vibration isolation, *J. Sound Vib.* 326 (2009) 88–103.
- [24] H. Fan, L. Yang, Y. Tian, Z. Wang, Design of metastructures with quasi-zero dynamic stiffness for vibration isolation, *Compos. Struct.* 243 (2020) 112244.
- [25] G. Jiang, X. Jing, Y. Guo, A novel bio-inspired multi-joint anti-vibration structure and its nonlinear HSLDS properties, *Mech. Syst. Sig. Process.* 138 (2020) 106552.
- [26] J. Bian, X. Jing, Superior nonlinear passive damping characteristics of the bio-inspired limb-like or X-shaped structure, *Mech. Syst. Sig. Process.* 125 (2019) 21–51.
- [27] X. Tan, S. Chen, S. Zhu, B. Wang, P. Xu, K. Yao, Y. Sun, Reusable metamaterial via inelastic instability for energy absorption, *Int. J. Mech. Sci.* 155 (2019) 509–517.
- [28] A. Rafsanjani, A. Akbarzadeh, D. Pasini, Snapping Mechanical Metamaterials under Tension, *Adv. Mater.* 27 (2015) 5931–5935.
- [29] D. Restrepo, N.D. Mankame, P.D. Zavattieri, Phase transforming cellular materials, *Extreme Mech. Lett.* 4 (2015) 52–60.
- [30] Q. Luo, L. Tong, Optimal Design of Bi-and Multi-Stable Compliant Cellular Structures, ASME 2018 International Design Engineering Technical Conferences and Computers and Information in Engineering Conference, American Society of Mechanical Engineers, 2018, pp. V05AT07A009-V005AT007A009.
- [31] S. Liu, A.I. Azad, R. Burgueño, Architected materials for tailororable shear behavior with energy dissipation, *Extreme Mech. Lett.* 28 (2019) 1–7.
- [32] X. Tan, S. Chen, B. Wang, S. Zhu, L. Wu, Y. Sun, Design, fabrication, and characterization of multistable mechanical metamaterials for trapping energy, *Extreme Mech. Lett.* 28 (2019) 8–21.

- [33] H. Yang, L. Ma, Multi-stable mechanical metamaterials by elastic buckling instability, *J. Mater. Sci.* 54 (2019) 3509–3526.
- [34] J. Mei, G. Ma, M. Yang, Z. Yang, W. Wen, P. Sheng, Dark acoustic metamaterials as super absorbers for low-frequency sound, *Nat. Commun.* 3 (2012) 1758.
- [35] D. Del Vescovo, I. Giorgio, Dynamic problems for metamaterials: Review of existing models and ideas for further research, *Int. J. Eng. Sci.* 80 (2014) 153–172.
- [36] M.H. Fu, O.T. Xu, L.L. Hu, T.X. Yu, Nonlinear shear modulus of re-entrant hexagonal honeycombs under large deformation, *Int. J. Solids Struct.* 80 (2016) 284–296.
- [37] J. Bauer, L.R. Meza, T.A. Schaedler, R. Schwaiger, X. Zheng, L. Valdevit, Nanolattices: An Emerging Class of Mechanical Metamaterials, *Adv. Mater.* 29 (2017) 1701850.
- [38] Z. Liu, X. Zhang, Y. Mao, Y.Y. Zhu, Z. Yang, C.T. Chan, P. Sheng, Locally resonant sonic materials, *Science* 289 (2000) 1734–1736.
- [39] D.R. Smith, J.B. Pendry, M.C.K. Wiltshire, Metamaterials and negative refractive index, *Science* 305 (2004) 788–792.
- [40] J.B. Pendry, Negative refraction makes a perfect lens, *Phys. Rev. Lett.* 85 (2000) 3966–3969.
- [41] R.A. Shelby, D.R. Smith, S. Schultz, Experimental verification of a negative index of refraction, *Science* 292 (2001) 77–79.
- [42] J.B. Pendry, D. Schurig, D.R. Smith, Controlling electromagnetic fields, *Science* 312 (2006) 1780–1782.
- [43] W. Cai, U.K. Chettiar, A.V. Kildishev, V.M. Shalaev, Optical cloaking with metamaterials, *Nat. Photonics* 1 (2007) 224–227.
- [44] M.R. Haberman, M.D. Guild, Acoustic metamaterials, *Phys. Today* 69 (2016) 42–48.
- [45] T.A. Schaedler, W.B. Carter, Architected Cellular Materials, *Annu. Rev. Mater. Res.* (2016) 187–210.
- [46] A.A. Zadpoor, Mechanical meta-materials, *Mater. Horiz.* 3 (2016) 371–381.
- [47] X. Ren, R. Das, P. Tran, T.D. Ngo, Y.M. Xie, Auxetic metamaterials and structures: A review, *Smart Mater. Struct.* 27 (2018) 023001.
- [48] J.U. Surjadi, L. Gao, H. Du, X. Li, X. Xiong, N.X. Fang, Y. Lu, Mechanical Metamaterials and Their Engineering Applications, *Adv. Eng. Mater.* 21 (2019) 1800864.
- [49] B. Gramüller, J. Boblenz, C. Hühne, PACS – Realization of an adaptive concept using pressure actuated cellular structures, *Smart Mater. Struct.* 23 (2014) 115006.
- [50] G.L. Huang, C.T. Sun, Band gaps in a multiresonator acoustic metamaterial, *J. Vibrat. Acoust., Trans. ASME* 132 (2010) 0310031–0310036.
- [51] P.F. Pai, Metamaterial-based broadband elastic wave absorber, *J. Intell. Mater. Syst. Struct.* 21 (2010) 517–528.
- [52] M. Reynolds, S. Daley, Enhancing the band gap of an active metamaterial, *J. Vib. Control* 23 (2017) 1782–1791.
- [53] T. Bückmann, N. Stenger, M. Kadic, J. Kaschke, A. Fröhlich, T. Kennerknecht, C. Eberl, M. Thiel, M. Wegener, Tailored 3D mechanical metamaterials made by dip-in direct-laser-writing optical lithography, *Adv. Mater.* 24 (2012) 2710–2714.
- [54] S. Babaei, J. Shim, J.C. Weaver, E.R. Chen, N. Patel, K. Bertoldi, 3D soft metamaterials with negative poisson's ratio, *Adv. Mater.* 25 (2013) 5044–5049.
- [55] K.K. Saxena, R. Das, E.P. Calius, Three Decades of Auxetics Research – Materials with Negative Poisson's Ratio: A Review, *Adv. Eng. Mater.* 18 (2016) 1847–1870.
- [56] A. Martin, M. Kadic, R. Schittny, T. Bückmann, M. Wegener, Phonon band structures of three-dimensional pentamode metamaterials, *Phys. Rev. B – Condens. Matter Mater. Phys.* 86 (2012) 155116.
- [57] M. Kadic, T. Bückmann, R. Schittny, M. Wegener, On anisotropic versions of three-dimensional pentamode metamaterials, *New J. Phys.* 15 (2013) 023029.
- [58] T. Bückmann, M. Thiel, M. Kadic, R. Schittny, M. Wegener, An elasto-mechanical unfeelability cloak made of pentamode metamaterials, *Nat. Commun.* 5 (2014) 4130.
- [59] S. Li, H. Fang, S. Sadeghi, P. Bhowad, K.W. Wang, Architected Origami Materials: How Folding Creates Sophisticated Mechanical Properties, *Adv. Mater.* 31 (2019) e1805282.
- [60] H. Fang, S.C.A. Chu, Y. Xia, K.W. Wang, Programmable Self-Locking Origami Mechanical Metamaterials, *Adv. Mater.* 30 (2018) 1706311.
- [61] A. Gillman, K. Fuchi, P.R. Buskohl, Truss-based nonlinear mechanical analysis for origami structures exhibiting bifurcation and limit point instabilities, *Int. J. Solids Struct.* 147 (2018) 80–93.
- [62] J. Ma, J. Song, Y. Chen, An origami-inspired structure with graded stiffness, *Int. J. Mech. Sci.* 136 (2018) 134–142.
- [63] H.H. Huang, C.T. Sun, Wave attenuation mechanism in an acoustic metamaterial with negative effective mass density, *New J. Phys.* 11 (2009) 013003.
- [64] M.H. Lu, L. Feng, Y.F. Chen, Phononic crystals and acoustic metamaterials, *Mater. Today* 12 (2009) 34–42.
- [65] Z. Yang, H.M. Dai, N.H. Chan, G.C. Ma, P. Sheng, Acoustic metamaterial panels for sound attenuation in the 50–1000 Hz regime, *Appl. Phys. Lett.* 96 (2010) 041906.
- [66] N.I. Zheludev, The road ahead for metamaterials, *Science* 328 (2010) 582–583.
- [67] C.M. Soukoulis, M. Wegener, Past achievements and future challenges in the development of three-dimensional photonic metamaterials, *Nat. Photonics* 5 (2011) 523–530.
- [68] M.I. Hussein, M.J. Leamy, M. Ruzzene, Dynamics of phononic materials and structures: Historical origins, recent progress, and future outlook, *Appl. Mech. Rev.* 66 (2014) 040802.
- [69] S.A. Cummer, J. Christensen, A. Alù, Controlling sound with acoustic metamaterials, *Nat. Rev. Mater.* 1 (2016) 16001.
- [70] S. Cortes, J. Allison, C. Morris, M.R. Haberman, C.C. Seepersad, D. Kovar, Design, Manufacture, and Quasi-Static Testing of Metallic Negative Stiffness Structures within a Polymer Matrix, *Exp. Mech.* 57 (2017) 1183–1191.
- [71] X. Zheng, W. Smith, J. Jackson, B. Moran, H. Cui, D. Chen, J. Ye, N. Fang, N. Rodriguez, T. Weisgraber, C.M. Spadaccini, Multiscale metallic metamaterials, *Nat. Mater.* 15 (2016) 1100–1106.
- [72] X. Tan, B. Wang, S. Zhu, S. Chen, K. Yao, P. Xu, L. Wu, Y. Sun, Novel multidirectional negative stiffness mechanical metamaterials, *Smart Mater. Struct.* 29 (2020) 015037.
- [73] L.R. Meza, G.P. Philpot, C.M. Portela, A. Maggi, L.C. Montemayor, A. Comella, D.M. Kochmann, J.R. Greer, Reexamining the mechanical property space of three-dimensional lattice architectures, *Acta Mater.* 140 (2017) 424–432.
- [74] C. Lv, D. Krishnaraju, G. Konjevod, H. Yu, H. Jiang, Origami based mechanical metamaterials, *Sci. Rep.* 4 (2014) 5979.
- [75] M. Schenk, S.D. Guest, Geometry of Miura-folded metamaterials, *Proc. Natl. Acad. Sci.* 110 (2013) 3276–3281.
- [76] E.A. Peraza-Hernandez, D.J. Hartl, R.J. Malak Jr, D.C. Lagoudas, Origami-inspired active structures: a synthesis and review, *Smart Mater. Struct.* 23 (2014) 094001.
- [77] J.L. Silverberg, A.A. Evans, L. McLeod, R.C. Hayward, T. Hull, C.D. Santangelo, I. Cohen, Using origami design principles to fold reprogrammable mechanical metamaterials, *Science* 345 (2014) 647–650.
- [78] R.J. Lang, Origami: Complexity in creases, again, *Engineering and Science* 67 (2004) 5–19.
- [79] Y. Hu, H. Liang, H. Duan, Design of Cylindrical and Axisymmetric Origami Structures Based on Generalized Miura-Ori Cell, *Journal of Mechanisms and Robotics* 11 (2019) 051004.
- [80] M. Thota, K.W. Wang, Reconfigurable origami sonic barriers with tunable bandgaps for traffic noise mitigation, *J. Appl. Phys.* 122 (2017) 154901.
- [81] M. Thota, K.W. Wang, Tunable waveguiding in origami phononic structures, *J. Sound Vib.* 430 (2018) 93–100.
- [82] L.H. Dudit, E. Vouga, T. Tachi, L. Mahadevan, Programming Curvature using Origami Tessellations, *Nat. Mater.* 15 (2018) 583–588.
- [83] E.A.P. Hernandez, D.J. Hartl, D.C. Lagoudas, Active Origami: Modeling, Design, and Applications, Springer, 2018.
- [84] S. Barbarino, O. Bilgen, R.M. Ajaj, M.I. Friswell, D.J. Inman, A Review of Morphing Aircraft, *J. Intell. Mater. Syst. Struct.* 22 (2011) 823–877.
- [85] X. Lachenal, S. Daynes, P.M. Weaver, Review of morphing concepts and materials for wind turbine blade applications, *Wind Energy* 16 (2013) 283–307.
- [86] E. Morris, McAdams, Daniel A., and Malak, Richard., The State of the Art of Origami-Inspired Products: A Review, Proceedings of the ASME 2016 International Design Engineering Technical Conferences and Computers and Information in Engineering Conference, Charlotte, North Carolina, USA, 2016, pp. V05BT07A014.

- [87] A. M. Willis, Collapsible kayak, (2012) US 8,316,788 B2.
- [88] R.V. Martinez, C.R. Fish, X. Chen, G.M. Whitesides, Elastomeric origami: programmable paper-elastomer composites as pneumatic actuators, *Adv. Funct. Mater.* 22 (2012) 1376–1384.
- [89] A. Heller, A giant leap for space telescopes, *Sci. Technol. Rev.* (2003) 12–18.
- [90] B.P. DeFigueiredo, N.A. Pehrson, K.A. Tolman, E. Crampton, S.P. Magleby, L.L. Howell, Origami-Based Design of Conceal-and-Reveal Systems, *J. Mechan. Robot.* 11 (2019) 020904.
- [91] J. Butler, L. Bowen, E. Wilcox, A. Shrager, M.I. Frecker, P. von Lockette, T.W. Simpson, R.J. Lang, L.L. Howell, S.P. Magleby, A Model for Multi-Input Mechanical Advantage in Origami-Based Mechanisms, *J. Mechan. Robot.* 10 (2018) 061007.
- [92] J. Ma, Z. You, Energy Absorption of Thin-Walled Square Tubes With a Prefolded Origami Pattern—Part I: Geometry and Numerical Simulation, *J. Appl. Mech. Trans. ASME* 81 (2014) 011003.
- [93] K. Yang, S. Xu, J. Shen, S. Zhou, Y.M. Xie, Energy absorption of thin-walled tubes with pre-folded origami patterns: Numerical simulation and experimental verification, *Thin-Walled Struct.* 103 (2016) 33–44.
- [94] B. Sargent, J. Butler, K. Seymour, D. Bailey, B. Jensen, S. Magleby, L. Howell, An Origami-Based Medical Support System to Mitigate Flexible Shaft Buckling, *J. Mechan. Robot.* 12 (2020) 041005.
- [95] H. Banerjee, T.K. Li, G. Ponraj, S.K. Kirithika, C.M. Lim, H. Ren, Origami-Layer-Jamming Deployable Surgical Retractor With Variable Stiffness and Tactile Sensing, *J. Mechan. Robot.* 12 (2020) 031010.
- [96] A.J. Taylor, Y. Chen, M. Fok, A. Berman, K. Nilsson, Z.T. Ho Tse, Cardiovascular Catheter With an Expandable Origami Structure, *J. Med. Devices* 11 (2017) 034505.
- [97] D. Rus, M.T. Tolley, Design, fabrication and control of origami robots, *Nat. Rev. Mater.* 3 (2018) 101–112.
- [98] A. Firouzeh, J. Paik, Robogami: a Fully Integrated Low-Profile Robotic Origami, *J. Mechan. Robot.* 7 (2015) 021009.
- [99] H. Banerjee, N. Pusalkar, H. Ren, Single-Motor Controlled Tendon-Driven Peristaltic Soft Origami Robot, *J. Mechan. Robot.* 10 (2018) 064501.
- [100] A.F. Arrieta, O. Bilgen, M.I. Friswell, P. Hagedorn, Dynamic control for morphing of bi-stable composites, *J. Intell. Mater. Syst. Struct.* 24 (2012) 266–273.
- [101] S. Waitukaitis, R. Menaut, B.G.G. Chen, M. van Hecke, Origami multistability: From single vertices to metasheets, *Phys. Rev. Lett.* 114 (2015) 055503.
- [102] T. Tachi, T.C. Hull, Self-Foldability of Rigid Origami, *J. Mechan. Robot.* 9 (2017) 021008.
- [103] K.C. Cheung, T. Tachi, S. Calisch, K. Miura, Origami interleaved tube cellular materials, *Smart Mater. Struct.* 23 (2014) 094012.
- [104] X. Yu, J. Zhou, H. Liang, Z. Jiang, L. Wu, Mechanical metamaterials associated with stiffness, rigidity and compressibility: A brief review, *Prog. Mater. Sci.* 94 (2018) 114–173.
- [105] S.P. Timoshenko, J.M. Gere, *Theory of elasticity*, McGraw-Hill, New York, 1970.
- [106] G.W. Milton, Composite materials with poisson's ratios close to -1, *J. Mech. Phys. Solids* 40 (1992) 1105–1137.
- [107] G.W. Milton, A.V. Cherkashev, Which elasticity tensors are realizable?, *J. Eng. Mater. Technol., Trans. ASME* 117 (1995) 483–493.
- [108] S. Yao, X. Zhou, G. Hu, Experimental study on negative effective mass in a 1D mass-spring system, *New J. Phys.* 10 (2008) 043020.
- [109] J. Valentine, J. Li, T. Zentgraf, G. Bartal, X. Zhang, An optical cloak made of dielectrics, *Nat. Mater.* 8 (2009) 568–571.
- [110] R.S. Lakes, T. Lee, A. Bersie, Y.C. Wang, Extreme damping in composite materials with negative-stiffness inclusions, *Nature* 410 (2001) 565–567.
- [111] T. Klatt, M.R. Haberman, A nonlinear negative stiffness metamaterial unit cell and small-on-large multiscale material model, *J. Appl. Phys.* 114 (2013) 033503.
- [112] G. Ma, P. Sheng, Acoustic metamaterials: From local resonances to broad horizons, *Sci. Adv.* 2 (2016) e1501595.
- [113] R. Lakes, K.W. Wojciechowski, Negative compressibility, negative Poisson's ratio, and stability, *Phys. Status Solidi (B) Basic Res.* 245 (2008) 545–551.
- [114] J. Bunyan, S. Tawfick, Exploiting Structural Instability to Design Architected Materials Having Essentially Nonlinear Stiffness, *Adv. Eng. Mater.* 21 (2019) 1800791.
- [115] K. Virk, A. Monti, T. Trehard, M. Marsh, K. Hazra, K. Boba, C.D.L. Remillat, F. Scarpa, I.R. Farrow, SILICOMB PEEK Kirigami cellular structures: Mechanical response and energy dissipation through zero and negative stiffness, *Smart Mater. Struct.* 22 (2013) 084014.
- [116] K. Che, C. Yuan, J. Wu, H.J. Qi, J. Meaud, Three-dimensional-printed multistable mechanical metamaterials with a deterministic deformation sequence, *J. Appl. Mechan., Trans. ASME* 84 (2017) 011004.
- [117] D. Chronopoulos, I. Antoniadis, T. Ampatzidis, Enhanced acoustic insulation properties of composite metamaterials having embedded negative stiffness inclusions, *Extreme Mech. Lett.* 12 (2017) 48–54.
- [118] B.M. Goldsberry, M.R. Haberman, Negative stiffness honeycombs as tunable elastic metamaterials, *J. Appl. Phys.* 123 (2018) 091711.
- [119] C.S. Ha, R.S. Lakes, M.E. Plesha, Design, fabrication, and analysis of lattice exhibiting energy absorption via snap-through behavior, *Mater. Des.* 141 (2018) 426–437.
- [120] Z. Hashin, S. Shtrikman, A variational approach to the theory of the elastic behaviour of multiphase materials, *J. Mech. Phys. Solids* 11 (1963) 127–140.
- [121] S. Hyun, S. Torquato, Optimal and manufacturable two-dimensional, Kagomé-like cellular solids, *J. Mater. Res.* 17 (2002) 137–144.
- [122] J.B. Berger, H.N.G. Wadley, R.M. McMeeking, Mechanical metamaterials at the theoretical limit of isotropic elastic stiffness, *Nature* 543 (2017) 533–537.
- [123] Q. Luo, L. Tong, Adaptive pressure-controlled cellular structures for shape morphing I: design and analysis, *Smart Mater. Struct.* 22 (2013) 055014.
- [124] Q. Luo, L. Tong, Adaptive pressure-controlled cellular structures for shape morphing: II. Numerical and experimental validation, *Smart Mater. Struct.* 22 (2013) 055015.
- [125] J. Lv, L. Tang, W. Li, L. Liu, H. Zhang, Topology optimization of adaptive fluid-actuated cellular structures with arbitrary polygonal motor cells, *Smart Mater. Struct.* 25 (2016) 055021.
- [126] T. Tancogne-Dejean, M. Diamantopoulou, M.B. Gorji, C. Bonatti, D. Mohr, 3D Plate-Lattices: An Emerging Class of Low-Density Metamaterial Exhibiting Optimal Isotropic Stiffness, *Adv. Mater.* 30 (2018) 180334.
- [127] M. Alfouneh, J. Ji, Q. Luo, Optimal design of multi-cellular cores for sandwich panels under harmonic excitation, *Compos. Struct.* 248 (2020) 112507.
- [128] L.J. Gibson, Biomechanics of cellular solids, *J. Biomech.* 38 (2005) 377–399.
- [129] L.R. Meza, A.J. Zelhofer, N. Clarke, A.J. Mateos, D.M. Kochmann, J.R. Greer, Resilient 3D hierarchical architected metamaterials, *Proceed. Natl. Acad. Sci. USA*, 112 (2015) 11502–11507.
- [130] J. Bauer, A. Schroer, R. Schwaiger, O. Kraft, Approaching theoretical strength in glassy carbon nanolattices, *Nat. Mater.* 15 (2016) 438–443.
- [131] Y. Li, E. Baker, T. Reissman, C. Sun, W.K. Liu, Design of mechanical metamaterials for simultaneous vibration isolation and energy harvesting, *Appl. Phys. Lett.* 111 (2017) 251903.
- [132] D.A. Debeau, C.C. Seepersad, M.R. Haberman, Impact behavior of negative stiffness honeycomb materials, *J. Mater. Res.* 33 (2018) 290–299.
- [133] A. Sridhar, L. Liu, V.G. Kouznetsova, M.G.D. Geers, Homogenized enriched continuum analysis of acoustic metamaterials with negative stiffness and double negative effects, *J. Mech. Phys. Solids* 119 (2018) 104–117.
- [134] C. Bonatti, D. Mohr, Mechanical performance of additively-manufactured anisotropic and isotropic smooth shell-lattice materials: Simulations & experiments, *J. Mech. Phys. Solids* 122 (2019) 1–26.
- [135] N. Cohen, R.M. McMeeking, M.R. Begley, Modeling the non-linear elastic response of periodic lattice materials, *Mech. Mater.* 129 (2019) 159–168.
- [136] F. Robert, An isotropic three-dimensional structure with Poisson's ratio =-1, *J. Elast.* 15 (1985) 427–430.
- [137] R. Lakes, Foam structures with a negative poisson's ratio, *Science* 235 (1987) 1038–1040.
- [138] L. Rothenburg, A.A. Berlin, R.J. Bathurst, Microstructure of isotropic materials with negative Poisson's ratio, *Nature* 354 (1991) 470–472.
- [139] F. Scarpa, L.G. Ciffo, J.R. Yates, Dynamic properties of high structural integrity auxetic open cell foam, *Smart Mater. Struct.* 13 (2004) 49–56.

- [140] Y. Prawoto, Seeing auxetic materials from the mechanics point of view: A structural review on the negative Poisson's ratio, *Comput. Mater. Sci.* 58 (2012) 140–153.
- [141] T.A.M. Hewage, K.L. Alderson, A. Alderson, F. Scarpa, Double-Negative Mechanical Metamaterials Displaying Simultaneous Negative Stiffness and Negative Poisson's Ratio Properties, *Adv. Mater.* 28 (2016) 10323–10332.
- [142] C. Huang, L. Chen, Negative Poisson's Ratio in Modern Functional Materials, *Adv. Mater.* (2016) 8079–8096.
- [143] L. Yang, O. Harrysson, H. West, D. Cormier, Mechanical properties of 3D re-entrant honeycomb auxetic structures realized via additive manufacturing, *Int. J. Solids Struct.* 69–70 (2015) 475–490.
- [144] D. Li, L. Dong, J. Yin, R.S. Lakes, Negative Poisson's ratio in 2D Voronoi cellular solids by biaxial compression: a numerical study, *J. Mater. Sci.* 51 (2016) 7029–7037.
- [145] M.H. Fu, Y. Chen, LL. Hu, A novel auxetic honeycomb with enhanced in-plane stiffness and buckling strength, *Compos. Struct.* 160 (2017) 574–585.
- [146] A. Ingole, A. Hao, R. Liang, Design and modeling of auxetic and hybrid honeycomb structures for in-plane property enhancement, *Mater. Des.* 117 (2017) 72–83.
- [147] H.M.A. Kolken, A.A. Zadpoor, Auxetic mechanical metamaterials, *RSC Adv.* 7 (2017) 5111–5129.
- [148] R.S. Lakes, Negative-Poisson's-Ratio Materials: Auxetic Solids, *Annu. Rev. Mater. Res.* (2017) 63–81.
- [149] K.K. Dudek, R. Gatt, M.R. Dudek, J.N. Grima, Negative and positive stiffness in auxetic magneto-mechanical metamaterials, *Proceed. Roy. Soc. A: Mathemat., Phys. Eng. Sci.* 474 (2018) 20180003.
- [150] T. Li, Y. Chen, X. Hu, Y. Li, L. Wang, Exploiting negative Poisson's ratio to design 3D-printed composites with enhanced mechanical properties, *Mater. Des.* 142 (2018) 247–258.
- [151] X. Ren, J. Shen, P. Tran, T.D. Ngo, Y.M. Xie, Auxetic nail: Design and experimental study, *Compos. Struct.* 184 (2018) 288–298.
- [152] X. Ren, J. Shen, P. Tran, T.D. Ngo, Y.M. Xie, Design and characterisation of a tuneable 3D buckling-induced auxetic metamaterial, *Mater. Des.* 139 (2018) 336–342.
- [153] Y.L. Chen, X.T. Wang, L. Ma, Damping mechanisms of CFRP three-dimensional double-arrow-head auxetic metamaterials, *Polym. Test.* 81 (2020) 106189.
- [154] A. Rafsanjani, D. Pasini, Bistable auxetic mechanical metamaterials inspired by ancient geometric motifs, *Extreme Mech. Lett.* 9 (2016) 291–296.
- [155] H. Qin, D. Yang, Vibration reduction design method of metamaterials with negative Poisson's ratio, *J. Mater. Sci.* 54 (2019) 14038–14054.
- [156] Q. Li, D. Yang, Vibro-acoustic performance and design of annular cellular structures with graded auxetic mechanical metamaterials, *J. Sound Vib.* 466 (2020) 115038.
- [157] C. Croënne, E.J.S. Lee, H. Hu, J.H. Page, Band gaps in phononic crystals: Generation mechanisms and interaction effects, *AIP Adv.* 1 (2011) 041401.
- [158] M. Ruzzene, F. Scarpa, F. Soranna, Wave beaming effects in two-dimensional cellular structures, *Smart Mater. Struct.* 12 (2003) 363–372.
- [159] X. Xu, M.V. Barnhart, X. Li, Y. Chen, G. Huang, Tailoring vibration suppression bands with hierarchical metamaterials containing local resonators, *J. Sound Vib.* 442 (2019) 237–248.
- [160] L. D'Alessandro, R. Ardito, F. Braghin, A. Corigliano, Low frequency 3D ultra-wide vibration attenuation via elastic metamaterial, *Sci. Rep.* 9 (2019) 8039.
- [161] M.H. Bae, J.H. Oh, Amplitude-induced bandgap: New type of bandgap for nonlinear elastic metamaterials, *J. Mech. Phys. Solids* 139 (2020) 103930.
- [162] Z. Wu, K.W. Wang, On the wave propagation analysis and supratransmission prediction of a metastable modular metastructure for non-reciprocal energy transmission, *J. Sound Vib.* 458 (2019) 389–406.
- [163] X. Liu, G. Cai, K.W. Wang, Synthesizing and reconfiguring metastable modular metamaterials for adaptive wave propagation control, *J. Sound Vib.* 468 (2020) 115114.
- [164] R.K. Narisetti, M.J. Leamy, M. Ruzzene, A perturbation approach for predicting wave propagation in one-dimensional nonlinear periodic structures, *J. Vibrat. Acoust., Trans. ASME* 132 (2010) 0310011–03100111.
- [165] G. Gantzounis, M. Serra-Garcia, K. Homma, J.M. Mendoza, C. Daraio, Granular metamaterials for vibration mitigation, *J. Appl. Phys.* 114 (2013) 093514.
- [166] I.L. Chang, Z.X. Liang, H.W. Kao, S.H. Chang, C.Y. Yang, The wave attenuation mechanism of the periodic local resonant metamaterial, *J. Sound Vib.* 412 (2018) 349–359.
- [167] R. Zhu, X.N. Liu, G.K. Hu, C.T. Sun, G.L. Huang, Negative refraction of elastic waves at the deep-subwavelength scale in a single-phase metamaterial, *Nat. Commun.* 5 (2014) 5510.
- [168] R. Zhu, X.N. Liu, G.K. Hu, C.T. Sun, G.L. Huang, A chiral elastic metamaterial beam for broadband vibration suppression, *J. Sound Vib.* 333 (2014) 2759–2773.
- [169] S.C. Han, J.W. Lee, K. Kang, A New Type of Low Density Material: Shellular, *Adv. Mater.* 27 (2015) 5506–5511.
- [170] K. H. Matlack, A. Bauhofer, S. Krödel, A. Palermo, C. Daraio, Composite 3D-printed metastructures for low frequency and broadband vibration absorption, *Proceed. Natl. Acad. Sci. USA*, 113 (2016) 8386–8390.
- [171] Z. Wang, Q. Zhang, K. Zhang, G. Hu, Tunable Digital Metamaterial for Broadband Vibration Isolation at Low Frequency, *Adv. Mater.* 28 (2016) 9857–9861.
- [172] M.C. Messner, Optimal lattice-structured materials, *J. Mech. Phys. Solids* 96 (2016) 162–183.
- [173] C. Sugino, S. Leadenhurst, M. Ruzzene, A. Erturk, On the mechanism of bandgap formation in locally resonant finite elastic metamaterials, *J. Appl. Phys.* 120 (2016) 134501.
- [174] R.L. Harne, D.C. Urbaneck, Enhancing broadband vibration energy suppression using local buckling modes in constrained metamaterials, *J. Vibrat., Trans. ASME* 139 (2017) 061004.
- [175] H.J. Xiang, Z.F. Shi, S.J. Wang, Y.L. Mo, Periodic materials-based vibration attenuation in layered foundations: Experimental validation, *Smart Mater. Struct.* 21 (2012) 112003.
- [176] H. Al Ba'ba'a, M. Nouh, T. Singh, Formation of local resonance band gaps in finite acoustic metamaterials: A closed-form transfer function model, *J. Sound Vib.* 410 (2017) 429–446.
- [177] A.O. Krushynska, M. Miniaci, F. Bosia, N.M. Pugno, Coupling local resonance with Bragg band gaps in single-phase mechanical metamaterials, *Extreme Mech. Lett.* 12 (2017) 30–36.
- [178] S. Brûlé, E.H. Javelaud, S. Enoch, S. Guenneau, Experiments on seismic metamaterials: Molding surface waves, *Phys. Rev. Lett.* 112 (2013) 133901.
- [179] Y. Chen, G. Huang, C. Sun, Band gap control in an active elastic metamaterial with negative capacitance piezoelectric shunting, *J. Vib. Acoust.* 136 (2014) 061008.
- [180] C.J. Naify, C.M. Chang, G. McKnight, S. Nutt, Transmission loss and dynamic response of membrane-type locally resonant acoustic metamaterials, *J. Appl. Phys.* 108 (2010) 114905.
- [181] X. Fang, J. Wen, B. Bonello, J. Yin, D. Yu, Ultra-low and ultra-broad-band nonlinear acoustic metamaterials, *Nat. Commun.* 8 (2017) 1288.
- [182] T. Jiang, Q. He, Dual-directionally tunable metamaterial for low-frequency vibration isolation, *Appl. Phys. Lett.* 110 (2017) 021907.
- [183] X. Xu, M.V. Barnhart, X. Fang, J. Wen, Y. Chen, G. Huang, A nonlinear dissipative elastic metamaterial for broadband wave mitigation, *Int. J. Mech. Sci.* 164 (2019) 105159.
- [184] A.O. Krushynska, A. Amendola, F. Bosia, C. Daraio, N.M. Pugno, F. Fraternali, Accordion-like metamaterials with tunable ultra-wide low-frequency band gaps, *New J. Phys.* 20 (2018) 073051.
- [185] Z. Wu, F. Li, C. Zhang, Band-gap analysis of a novel lattice with a hierarchical periodicity using the spectral element method, *J. Sound Vib.* 421 (2018) 246–260.
- [186] K. Wang, J. Zhou, D. Xu, H. Ouyang, Lower band gaps of longitudinal wave in a one-dimensional periodic rod by exploiting geometrical nonlinearity, *Mech. Syst. Sig. Process.* 124 (2019) 664–678.

- [187] Z. Wu, W. Liu, F. Li, C. Zhang, Band-gap property of a novel elastic metamaterial beam with X-shaped local resonators, *Mech. Syst. Sig. Process.* 134 (2019) 106357.
- [188] C. Cai, J. Zhou, L. Wu, K. Wang, D. Xu, H. Ouyang, Design and numerical validation of quasi-zero-stiffness metamaterials for very low-frequency band gaps, *Compos. Struct.* 236 (2020) 111862.
- [189] L. Wu, Y. Wang, Z. Zhai, Y. Yang, D. Krishnaraju, J. Lu, F. Wu, Q. Wang, H. Jiang, Mechanical metamaterials for full-band mechanical wave shielding, *Appl. Mater. Today* 20 (2020) 100671.
- [190] M. Kadic, T. Bückmann, N. Stenger, M. Thiel, M. Wegener, On the practicability of pentamode mechanical metamaterials, *Appl. Phys. Lett.* 100 (2012) 191901.
- [191] M. Kadic, T. Bückmann, R. Schittny, P. Gumbsch, M. Wegener, Pentamode metamaterials with independently tailored bulk modulus and mass density, *Phys. Rev. Appl.* 2 (2014) 054007.
- [192] Y. Tian, Q. Wei, Y. Cheng, Z. Xu, X. Liu, Broadband manipulation of acoustic wavefronts by pentamode metasurface, *Appl. Phys. Lett.* 107 (2015) 221906.
- [193] A. Amendola, G. Benzoni, F. Fraternali, Non-linear elastic response of layered structures, alternating pentamode lattices and confinement plates, *Compos. B Eng.* 115 (2017) 117–123.
- [194] F. Fraternali, A. Amendola, Mechanical modeling of innovative metamaterials alternating pentamode lattices and confinement plates, *J. Mech. Phys. Solids* 99 (2017) 259–271.
- [195] R. Hedayati, A.M. Leeflang, A.A. Zadpoor, Additively manufactured metallic pentamode meta-materials, *Appl. Phys. Lett.* 110 (2017) 091905.
- [196] A. Zhao, Z. Zhao, X. Zhang, X. Cai, L. Wang, T. Wu, H. Chen, Design and experimental verification of a water-like pentamode material, *Appl. Phys. Lett.* 110 (2017) 011907.
- [197] C. Cai, Z. Wang, Y. Chu, G. Liu, Z. Xu, The phononic band gaps of Bragg scattering and locally resonant pentamode metamaterials, *J. Phys. D Appl. Phys.* 50 (2017) 415105.
- [198] Y. Guo, T. Dekorsy, M. Hettich, Topological guiding of elastic waves in phononic metamaterials based on 2D pentamode structures, *Sci. Rep.* 7 (2017) 18043.
- [199] L. Zhang, B. Song, A. Zhao, R. Liu, L. Yang, Y. Shi, Study on mechanical properties of honeycomb pentamode structures fabricated by laser additive manufacturing: Numerical simulation and experimental verification, *Compos. Struct.* 226 (2019) 111199.
- [200] C. Cai, C. Han, J. Wu, Z. Wang, Q. Zhang, Tuning method of phononic band gaps of locally resonant pentamode metamaterials, *J. Phys. D Appl. Phys.* 52 (2019) 045601.
- [201] Q. Li, J.S. Vipperman, Three-dimensional pentamode acoustic metamaterials with hexagonal unit cells, *J. Acoust. Soc. Am.* 145 (2019) 1372–1377.
- [202] N. Turner, B. Goodwine, M. Sen, A review of origami applications in mechanical engineering, *Proceed. Institut. Mechan. Eng., Part C: J. Mechan. Eng. Sci.* 230 (2016) 2345–2362.
- [203] X. Ning, X. Wang, Y. Zhang, X. Yu, D. Choi, N. Zheng, D.S. Kim, Y. Huang, Y. Zhang, J.A. Rogers, Assembly of Advanced Materials into 3D Functional Structures by Methods Inspired by Origami and Kirigami: A Review, *Adv. Mater. Interfaces* 5 (2018) 1800284.
- [204] H. Fang, S. Li, K.W. Wang, Self-locking degree-4 vertex origami structures, *Proceed. Roy. Soc. A: Mathemat., Phys. Eng. Sci.* 472 (2016) 20160682.
- [205] H. Fang, S. Li, H. Ji, K.W. Wang, Uncovering the deformation mechanisms of origami metamaterials by introducing generic degree-four vertices, *Phys. Rev. E* 94 (2016) 043002.
- [206] K. Miura, Method of packaging and deployment of large membranes in space, The Institute of Space and Astronautical Science report, 618 (1985) 1–9.
- [207] M. Eidini, G.H. Paulino, Unraveling metamaterial properties in zigzag-base folded sheets, *Sci. Adv.* 1 (2015) e1500224.
- [208] M. Eidini, Zigzag-base folded sheet cellular mechanical metamaterials, *Extreme Mech. Lett.* 6 (2016) 96–102.
- [209] H. Fang, S. Li, H. Ji, K.W. Wang, Dynamics of a bistable Miura-origami structure, *Phys. Rev. E* 95 (2017) 052211.
- [210] S. Kamrava, D. Mousanezhad, H. Ebrahimi, R. Ghosh, A. Vaziri, Origami-based cellular metamaterial with auxetic, bistable, and self-locking properties, *Sci. Rep.* 7 (2017) 46046.
- [211] S. Sengupta, S. Li, Harnessing the anisotropic multistability of stacked-origami mechanical metamaterials for effective modulus programming, *J. Intell. Mater. Syst. Struct.* 29 (2018) 2933–2945.
- [212] S. Li, K.W. Wang, Fluidic origami: a plant-inspired adaptive structure with shape morphing and stiffness tuning, *Smart Mater. Struct.* 24 (2015) 105031.
- [213] H. Yasuda, J. Yang, Reentrant Origami-Based Metamaterials with Negative Poisson's Ratio and Bistability, *Phys. Rev. Lett.* 114 (2015) 185502.
- [214] H. Yasuda, C. Chong, E.G. Charalampidis, P.G. Kevrekidis, J. Yang, Formation of rarefaction waves in origami-based metamaterials, *Phys. Rev. E* 93 (2016) 043004.
- [215] B.H. Hanna, J.M. Lund, R.J. Lang, S.P. Magleby, L.L. Howell, Waterbomb base: a symmetric single-vertex bistable origami mechanism, *Smart Mater. Struct.* 23 (2014) 094009.
- [216] B.H. Hanna, S.P. Magleby, R.J. Lang, L.L. Howell, Force-Deflection Modeling for Generalized Origami Waterbomb-Base Mechanisms, *J. Appl. Mechan., Trans. ASME* 82 (2015) 081001.
- [217] C. Jianguo, D. Xiaowei, Z. Ya, F. Jian, T. Yongming, Bistable Behavior of the Cylindrical Origami Structure With Kresling Pattern, *J. Mechan. Design, Trans. ASME* 137 (2015) 061406.
- [218] F. John, J. R. COOKE, Natural twist buckling in shells: from the hawkmoth's bellows to the deployable Kresling-pattern and cylindrical Miura-ori, Proceedings of the 6th International Conference on Computation of Shell and Spatial Structures IASS-IACM 2008: "Spanning Nano to Mega", Ithaca, NY, USA, 2008.
- [219] J. Song, Y. Chen, G. Lu, Axial crushing of thin-walled structures with origami patterns, *Thin-Walled Structures* 54 (2012) 65–71.
- [220] X. Zhang, Y. Chen, Vertex-Splitting on a Diamond Origami Pattern, *J. Mechan. Robot.* 11 (2019) 031014.
- [221] J. Ma, D. Hou, Y. Chen, Z. You, Quasi-static axial crushing of thin-walled tubes with a kite-shape rigid origami pattern: Numerical simulation, *Thin-Walled Struct.* 100 (2016) 38–47.
- [222] M. Shi, Ma, Jiayao, Chen, Yan, and You, Zhong., Energy Absorption of Origami Crash Box: Numerical Simulation and Theoretical Analysis, Proceedings of the ASME 2018 International Design Engineering Technical Conferences and Computers and Information in Engineering Conference, Quebec City, Quebec, Canada, 2018, pp. V05BT07A065.
- [223] H. Zhang, B. Zhu, X. Zhang, Origami Kaleidocycle-Inspired Symmetric Multistable Compliant Mechanisms, *J. Mechan. Robot.* 11 (2019) 011009.
- [224] J. Cai, X. Deng, Y. Xu, J. Feng, Motion Analysis of a Foldable Barrel Vault Based on Regular and Irregular Yoshimura Origami, *J. Mechan. Robot.* 8 (2016) 021017.
- [225] M.J. Harrington, K. Razghandi, F. Ditsch, L. Guiducci, M. Rueggberg, J.W. Dunlop, P. Fratzl, C. Neinhuis, I. Burgert, Origami-like unfolding of hydro-actuated ice plant seed capsules, *Nat. Commun.* 2 (2011) 337.
- [226] S. Daynes, R.S. Trask, P.M. Weaver, Bio-inspired structural bistability employing elastomeric origami for morphing applications, *Smart Mater. Struct.* 23 (2014) 125011.
- [227] L. Zhou, A.E. Marras, C.E. Castro, H.-J. Su, Pseudorigid-Body Models of Compliant DNA Origami Mechanisms, *J. Mechan. Robot.* 8 (2016) 051013.
- [228] S. Magleby, L. Howell, A. Avila, J. Greenwood, Conceptualizing Stable States in Origami-Based Devices Using an Energy Visualization Approach, *J. Mechan. Design, Trans. ASME* 142 (2020) 093302.
- [229] E.D. Demaine, M.L. Demaine, D.A. Huffman, D. Koschitz, T. Tachi, Characterization of curved creases and rulings: Design and analysis of lens tessellations, *Origami* 6 (2015) 209–230.
- [230] M.A. Dias, L.H. Dudte, L. Mahadevan, C.D. Santangelo, Geometric mechanics of curved crease origami, *Phys. Rev. Lett.* 109 (2012) 114301.
- [231] S. Nagasawa, Y. Fukuzawa, T. Yamaguchi, S. Tsukatani, I. Katayama, Effect of crease depth and crease deviation on folding deformation characteristics of coated paperboard, *J. Mater. Process. Technol.* 140 (2003) 157–162.

- [232] J.S. Dai, F. Cannella, Stiffness characteristics of carton folds for packaging, *J. Mechan. Design, Trans. ASME* 130 (2008) 022305.
- [233] S. Nagasawa, M. Mohd Nasruddin Bin, Y. Shiga, Bending moment characteristics on repeated folding motion of coated paperboard scored by round-edge knife, *J. Adv. Mechan. Design, Syst. Manufact.* 5 (2011) 385–394.
- [234] K. Francis, J. Blanch, S. Magleby, L. Howell, Origami-like creases in sheet materials for compliant mechanism design, *Mech. Sci.* 4 (2013) 371–380.
- [235] B.D. Jensen, L.L. Howell, Bistable configurations of compliant mechanisms modeled using four links and translational joints, *J. Mech. Des.* 126 (2004) 657–666.
- [236] H. Greenberg, M.L. Gong, S.P. Magleby, L.L. Howell, Identifying links between origami and compliant mechanisms, *Mech. Sci.* 2 (2011) 217–225.
- [237] E.T. Filipov, Y. Zhu, A Bar and Hinge Model for Simulating Bistability in Origami Structures With Compliant Creases, *J. Mechanis. Robot.* 12 (2020) 021110.
- [238] E.A. Peraza Hernandez, D.J. Hartl, D.C. Lagoudas, Kinematics of Origami Structures With Smooth Folds, *J. Mechan. Robot.* 8 (2016) 061019.
- [239] E.A. Peraza Hernandez, D.J. Hartl, E. Akleman, D.C. Lagoudas, Modeling and analysis of origami structures with smooth folds, *CAD, Comput. Aided Design* 78 (2016) 93–106.
- [240] S.A. Zirbel, R.J. Lang, M.W. Thomson, D.A. Sigel, P.E. Walkemeyer, B.P. Trease, S.P. Magleby, L.L. Howell, Accommodating Thickness in Origami-Based Deployable Arrays, *J. Mechan. Design, Trans. ASME* 135 (2013) 111005.
- [241] T. Tachi, Rigid-foldable thick origami, *Origami* 5 (2011) 253–264.
- [242] B.J. Edmondson, Lang, Robert J., Magleby, Spencer P., and Howell, Larry L., An Offset Panel Technique for Thick Rigidly Foldable Origami, Proceedings of the ASME 2014 International Design Engineering Technical Conferences and Computers and Information in Engineering Conference, Buffalo, New York, USA, 2014, pp. V05BT08A054.
- [243] J.S. Ku, E.D. Demaine, Folding Flat Crease Patterns With Thick Materials, *J. Mechan. Robot.* 8 (2016) 031003.
- [244] L. Howell, S. Magleby, B. Ignaut, N. Brown, R.J. Lang, Rigidly Foldable Thick Origami Using Designed-Offset Linkages, *J. Mechan. Robot.* 12 (2020) 021106.
- [245] A. Yellowhorse, L.L. Howell, Creating Rigid Foldability to Enable Mobility of Origami-Inspired Mechanisms, *J. Mechan. Robot.* 8 (2016) 011011.
- [246] J.L. Silverberg, J.H. Na, A.A. Evans, B. Liu, T.C. Hull, C.D. Santangelo, R.J. Lang, R.C. Hayward, I. Cohen, Origami structures with a critical transition to bistability arising from hidden degrees of freedom, *Nat. Mater.* 14 (2015) 389–393.
- [247] W. Wu, Z. You, Modelling rigid origami with quaternions and dual quaternions, *Proceed. Roy. Soc. A Mathemat., Phys. Eng. Sci.* 466 (2010) 2155–2174.
- [248] Jianguo Cai, Yuting Zhang, Yixiang Xu, Ya Zhou, J. Feng, The Foldability of Cylindrical Foldable Structures Based on Rigid Origami, *J. Mechan. Design, Trans. ASME*, 138 (2016) 031401.
- [249] J. Cai, Y. Liu, R. Ma, J. Feng, Y. Zhou, Nonrigidly Foldability Analysis of Kresling Cylindrical Origami, *J. Mechan. Robot.* 9 (2017) 041018.
- [250] J. Rommers, G. Radaelli, J.L. Herder, Pseudo-Rigid-Body Modeling of a Single Vertex Compliant-Facet Origami Mechanism, *J. Mechan. Robot.* 9 (2017) 031009.
- [251] J. Rommers, G. Radaelli, J.L. Herder, A Design Tool for a Single Vertex Compliant-Facet Origami Mechanism Including Torsional Hinge Lines, *J. Mechan. Robot.* 9 (2017) 061015.
- [252] Y. Hongying, G. Zhen, Z. Di, L. Peng, Mechanical Characteristics of Origami Mechanism Based on Thin Plate Bending Theory, *J. Appl. Mechan., Trans. ASME* 86 (2019) 081008.
- [253] L. Zimmermann, T. Stanković, Rigid and Flat Foldability of a Degree-Four Vertex in Origami, *J. Mechan. Robot.* 12 (2020) 011004.
- [254] L. Zimmermann, K. Shea, T. Stanković, Conditions for Rigid and Flat Foldability of Degree-n Vertices in Origami, *J. Mechan. Robot.* 12 (2020) 011020.
- [255] C.-H. Chiang, Kinematics of spherical mechanisms, Cambridge University Press Cambridge, 1988.
- [256] S.E. Wilding, L.L. Howell, S.P. Magleby, Spherical lamina emergent mechanisms, *Mech. Mach. Theory* 49 (2012) 187–197.
- [257] L.A. Bowen, C.L. Grames, S.P. Magleby, L.L. Howell, R.J. Lang, A Classification of Action Origami as Systems of Spherical Mechanisms, *J. Mechan. Design, Trans. ASME* 135 (2013) 111008.
- [258] S. Liu, W. Lv, Y. Chen, G. Lu, Deployable Prismatic Structures With Rigid Origami Patterns, *J. Mechan. Robot.* 8 (2016) 031002.
- [259] S. Ishida, K. Suzuki, H. Shimosaka, Design and Experimental Analysis of Origami-Inspired Vibration Isolator With Quasi-Zero-Stiffness Characteristic, *J. Vib. Acoust.* 139 (2017) 051004.
- [260] S. Ishida, H. Uchida, H. Shimosaka, I. Hagiwara, Design and Numerical Analysis of Vibration Isolators With Quasi-Zero-Stiffness Characteristics Using Bistable Foldable Structures, *J. Vib. Acoust.* 139 (2017) 031015.
- [261] C. Jianguo, D. Xiaowei, Z. Yuting, F. Jian, Z. Ya, Folding Behavior of a Foldable Prismatic Mast With Kresling Origami Pattern, *J. Mechan. Robot.* 8 (2016) 031004.
- [262] N. Kidambi, K. Wang, Dynamics of Kresling origami deployment, *Phys. Rev. E* 101 (2020) 063003.
- [263] H. Fang, K.W. Wang, S. Li, Asymmetric energy barrier and mechanical diode effect from folding multi-stable stacked-origami, *Extreme Mech. Lett.* 17 (2017) 7–15.
- [264] S. Sadeghi, S. Li, Dynamic folding of origami by exploiting asymmetric bi-stability, *Extreme Mech. Lett.* 40 (2020) 100958.
- [265] H. Yasuda, M. Lee, J. Yang, Tunable Wave Dynamics in Origami-Based Mechanical Metamaterials, Proceedings of the ASME 2016 International Design Engineering Technical Conferences and Computers and Information in Engineering Conference, Charlotte, North Carolina, USA, 2016, pp. V05BT07A012.
- [266] S. Sengupta, S. Li, Multi-stability and variable stiffness of cellular solids designed based on origami patterns, *Proc. SPIE* 10164, Active and Passive Smart Structures and Integrated Systems 2017, 2017, pp. 1016426.
- [267] Y. Xia, H. Fang, K. W. Wang, Exploring the Dynamic Characteristics of Degree-4 Vertex Origami Metamaterials, Proceedings of the ASME 2017 Conference on Smart Materials, Adaptive Structures and Intelligent Systems, Snowbird, Utah, USA, 2017, pp. V002T003A018.
- [268] Y. Lv, Y. Zhang, N. Gong, Z.-X. Li, G. Lu, X. Xiang, On the out-of-plane compression of a Miura-ori patterned sheet, *Int. J. Mech. Sci.* 161 (2019) 105022.
- [269] C. Qiu, K. Zhang, J.S. Dai, Repelling-Screw Based Force Analysis of Origami Mechanisms, *J. Mechan. Robot.* 8 (2016) 031001.
- [270] S. Sadeghi, S. Li, Fluidic origami cellular structure with asymmetric quasi-zero stiffness for low-frequency vibration isolation, *Smart Mater. Struct.* 28 (2019) 065006.
- [271] K. Inamoto, S. Ishida, Improved Feasible Load Range and Its Effect on the Frequency Response of Origami-Inspired Vibration Isolators With Quasi-Zero-Stiffness Characteristics, *J. Vib. Acoust.* 141 (2019) 021004.
- [272] G. Meng, Z.-K. Peng, W.-M. Zhang, S. Wang, T. Tan, H. Yan, H.-X. Zou, G. Yan, Multi-Direction Vibration Isolator for Momentum Wheel Assemblies, *J. Vib. Acoust.* 142 (2020) 041007.
- [273] T.-H. Kwok, C.C.L. Wang, D. Deng, Y. Zhang, Y. Chen, Four-Dimensional Printing for Freeform Surfaces: Design Optimization of Origami and Kirigami Structures, *J. Mechan. Design, Trans. ASME* 137 (2015) 111413.
- [274] J. A. Romero, Diago, L. A., Nara, C., Shinoda, J., and Hagiwara, I., Norigami Folding Machines for Complex 3D Shapes Proceedings of the ASME 2016 International Design Engineering Technical Conferences and Computers and Information in Engineering Conference, Charlotte, North Carolina, USA, 2016, pp. V05BT07A030.
- [275] B. P. Rhoads, and Su, Hai-Jun., The Design and Fabrication of a Deformable Origami Wheel, Proceedings of the ASME 2016 International Design Engineering Technical Conferences and Computers and Information in Engineering Conference, Charlotte, North Carolina, USA, 2016, pp. V05BT07A021.
- [276] X. Zhao, and Hagiwara, Ichiro., Designing and Manufacturing a Super Excellent and Ultra-Cheap Energy Absorber by Origami Engineering, Proceedings of the ASME 2019 International Design Engineering Technical Conferences and Computers and Information in Engineering Conference, Anaheim, California, USA, 2019, pp. V05BT07A037.